Technical Report
TR-23-12
December 2023

Microstructure, crystallography and CSL grain boundaries in copper canisters for nuclear waste disposal

Joacim Hagström

SVENSK KÄRNBRÄNSLEHANTERING AB

SWEDISH NUCLEAR FUEL
AND WASTE MANAGEMENT CO

Box 3091, SE-169 03 Solna
Phone +46 8 459 84 00
skb.se

SVENSK KÄRNBRÄNSLEHANTERING

ISSN 1404-0344
SKB TR-23-12
ID 1999804
December 2023

Microstructure, crystallography and CSL grain boundaries in copper canisters for nuclear waste disposal

Joacim Hagström, Swerim AB

Abstract

This study aims at investigating the microstructure and crystallography with special attention to grain boundary disorientation distribution and coincidence site lattice (CSL) grain boundaries at different positions in the walls and lid in copper canisters for disposal of spent nuclear fuel. Additionally, information is given on grain sizes, crystallographic texture and distribution of crystallographic planes parallel to the outer surfaces of the canister.

The project was planned to give detailed and statistically sound data on CSL boundaries in the copper canister wall- and lid material. CSL boundaries are boundaries with special symmetry (and properties), and have atom positions in the boundary that fit to both grains. Additionally, information on local variations in the material in the thickness direction or at different positions in the cylinder was of interest. To meet these objectives very large through thickness area analyses were performed at several positions of the 50 mm wall and lid.

The information gained will be used for modelling long term properties, e.g. creep ductility and corrosion resistance.

It was found that the canister wall material was homogeneous and the variation in CSL fractions, grain sizes and crystallographic texture were not very large. Some variation in grain size and texture was found in the thickness direction in the canister wall.

The top-sealing lid material showed however significant differences in disorientation distribution, CSL fractions, grain size, and texture strength compared to the canister wall material. The canister wall material was completely recrystallised and did not show a lot low angle grain boundaries or other signs typical for deformed material. The lid material was not completely recrystallised and did show significant amounts of low angle boundaries. The CSL fraction analysis showed that the lid material contained similar fractions of Σ3 twin boundaries but significantly more of the Σ9 boundaries compared to the canister wall material. The grain size was larger in the lid, and the texture strength was lower, 2 times random compared to 5–7 times random in the canister wall.

The microstructure close to the canister wall outer surface (measured from surface to 5 mm depth) showed somewhat different properties compared to the centre and the material close to the inner surface. The texture analysis showed that <110> and <100> closed packed crystal planes were more frequent, and the frequency of extra-large grains were also higher i.e., grains with diameters over 500 μm.

Sammanfattning

Målsättningen med arbetet var att undersöka mikrostrukturen kristallografiskt i materialet i olika positioner i väggar och lock i kopparkapslar som ska användas för slutförvaring av använt kärnbränsle. Speciellt fokus var att undersöka korngränsernas natur med avseende på vinkelskillnader (disorientering) och geometri. Korngränser med speciell symmetri (och egenskaper) är gränser mellan korn där gränsen har atomer som passar i båda kornens gitter, ”coincidence site lattice (CSL) grain boundaries”. Utöver information om korngränser var det även möjligt att analysera kornstorlek, kristallografisk textur och vilka kristallografiska plan som var vanligast parallellt med ytterytorna.

Projektet planerades för att skapa mycket detaljerad information med statistiskt tillförlitliga resultat för andelen korngränser med speciella relationer (CSL) i kopparcylinderväggar och lock. Det var också viktigt att ta fram information om hur mikrostrukturen, texturen, korngränsernas natur, etc varierade i tjockleksriktningen i olika positioner i kopparkapseln. För att kunna analysera variationer i tjockleksriktningen gjordes analyser tvärs igenom tjockleken (50 mm), från innerytan till ytterytan.

Informationen som tagits fram i projektet ska användas i modeller för att beskriva långtidsegenskaperna i materialet, t.ex. med avseende på krypning och motstånd mot korrosion.

Resultaten visade att materialet i väggar har homogen mikrostruktur, och variationen i korngränsernas natur, kornstorleksfördelning och kristallografisk textur var små. Viss variation i kornstorlek och textur i tjockleksriktningen i kapselns väggar kunde beläggas.

Skillnaden mellan mikrostrukturen i locket och väggarna var desto större, och signifikanta skillnader i korngränsernas natur, andelen CSL gränser, kornstorlek och texturens styrka kunde ses. Kapselväggarnas mikrostruktur var helt rekristalliserade och innehöll mycket lite dislokationer och lågvinkelkorngränser. Materialet i locket var inte helt rekristalliserat utan innehöll mycket dislokationer och lågvinkelkorngränser som är typiskt för ett material som utsatts för plastisk deformation. Fraktionen av de vanligaste tvillingarna (Σ3) var liknande, medan fraktionen Σ9 korngränser var tydligt större i lockmaterialet. Kornstorleken var större i lockmaterialet, men texturens styrka var lägre. I locket var texturen ca 2 gånger (icke texturerat material) och i väggarna ca 5–7 gånger.

Mikrostrukturen nära ytterytan i cylinderväggarna, från ytan och ner till 5 mm djup hade något annorlunda karaktär jämfört med mikrostrukturen längre in i materialet, i centrum och närmare innerytan. Texturen var annorlunda med större andel tätpackade plan av typen <110> och <100> parallella med ytterytan. Andelen stora korn med diameter över 500 µm var också större i ytan jämfört med centrum.

Contents

1 Introduction

Grain boundaries have different properties, boundary energies, mobility, depending on disorientation and interception angle. Low angle grain boundaries (LAGB), random high angle grain boundaries (HAGB), and Coincident site lattice (CSL) boundaries all have special properties that are important in many aspects. CSL boundaries behave differently compared to random HAGBs for important mechanisms such as recrystallisation, grain growth, segregation, precipitation of particles and solute element content. These special grain boundaries have lower energy compared to random grain boundaries which have consequences for important material properties, for example corrosion resistance, toughness, high temperature mechanical properties and creep properties (Sutton and Balluffi 1998, Randle 2010). One special case is the interaction between phosphorus and grain boundaries in oxygen-free phosphorus copper (OFP-copper) which is the chosen canister material for spent nuclear fuel. It is well established that small additions of phosphorus to oxygen free pure copper (Cu-OF) improves the creep properties at low temperatures. With additions of about 120 at. ppm P, both the creep strength and the creep ductility are raised (Sandström and Lousada 2021). The improvement in creep strength is a relative increase of about 20 % in the interval 75 to 250 °C. It is possible to compute the segregation energies of P and S using density functional theory (DFT) (Lousada and Korzhavyi 2022) and it is therefore important to know the fractions of different CSL boundaries in the material to be able to make reliable calculations and in the end more accurate models.

One research area within materials science that deals with CSL boundaries is Grain Boundary Engineering (GBE) (Gottstein and Shvindlerman 1999, Hagström et al. 2015, Trimby 2009). Materials can be designed to get improved properties if special grain boundaries can be created, and the number of random high angle grain boundaries can be suppressed. The thermo-mechanical process can be optimised to give higher fractions of CSL boundaries giving better corrosion properties, high temperature properties and creep properties. The studies of grain boundaries have increased the understanding of the importance of grain boundaries for material properties. The purpose of this work was to analyse the microstructure, grain size, crystallographic texture and grain boundary distribution in different positions in the copper canisters for nuclear waste disposal in Sweden. The canister has not specifically been optimised by GBE, but the field of research on grain boundaries and the effect grain boundaries have on the material properties has enlightened the importance of detailed information to predict the mechanical properties and also sensitivity for corrosion mechanisms. Modelling of long-term properties can be enhanced if detailed information on grain boundary distributions is known, and especially the fractions of different CSL boundaries is valuable information. The production processes of the canisters were not optimised to have specific grain boundary distribution, but copper contains a lot of CSL boundaries and it is important for the modelling of creep properties to have accurate information about this.

This work presents data on grain size, crystallographic texture and grain boundaries including fractions of CSL boundaries. The data have been evaluated from analysis in a scanning electron microscope (SEM) using electron back-scattered diffraction (EBSD) data from very large areas (> 500 mm^2) through the complete wall thickness (50 mm) giving high quality and statistical accurate information.

1.1 Introduction to EBSD – grain size, grain boundaries, grain boundary distribution, CSL boundaries, crystallographic texture and phase fraction

EBSD is a SEM based technique that uses electron diffraction to identify crystalline phases and crystal orientations. EBSD analysis in a modern field-emission electron microscope (FEG SEM) with high spatial resolution can resolve very fine structures, the lateral resolution is 10–20 nm in copper with 15–20 kV electron acceleration voltage. The penetration depth for EBSD analysis is shallow, the effective signal originates very close to the surface, the diffraction is induced from 2–5 nm depth below the surface. The technique is diffraction based and very sensitive to mechanical damage of the crystal or surface contamination, the thin oxide that forms naturally on copper exposed to air does however not influence the analysis. The acquisition speed is very high in modern EBSD systems, in

recrystallised materials with normal grain size less than a millisecond is needed to collect the diffraction pattern and process the Kikuchi-pattern to retrieve phase and orientation. Commonly EBSD is a scanning technique where crystal orientation maps are built up from many individual measurements. The EBSD analyses in this work was typically acquired at high frequency, ≥ 2 000 Hz. The analyses were built from many individual orientation maps, over 300, that were stitched together and combined into one large EBSD crystal orientation map for subsequent processing of the data to get information on grain size, crystallographic texture and CSL boundaries.

1.1.1 Post-processing of data

The raw data from the analyses can be post-processed to give valuable information about grain size, grain boundaries, crystallographic texture and deformation state, etc. The raw data is never 100 % indexed, there will always be individual pixels i.e. in grain boundaries, phase boundaries or surface defects, that were not indexed. Non-indexed pixels can be assigned orientation data by a data cleaning process, and this was done for the data in this project. The cleaning of data was done using AZTEC Crystal software. The raw data contained commonly less than 1 % non-indexed points, mainly in grain boundaries. In Figure 1-1 an example of how the raw data looks like without any cleaning. EBSD data from one single EBSD map (from top-sealing material) is plotted in two ways, in Figure 1-2a crystallographic orientations are plotted using colours according to the inverse pole figure (IPF) and in b) grain boundaries are plotted.

Grain boundaries – Low angle grain boundaries (LAGB) are dislocation-built boundaries which are common in deformed structures but uncommon in recrystallised materials. High angle grain boundaries (HAGB) are boundaries that are only a few atom layers wide and separate crystals (grains) of different orientations. It is common to use 10° or 15° misorientation as a criterion to define the transition from LAGB to HAGB, in this case 10° was used (10° will be used in this report if nothing else is stated). Random HAGB are boundaries between crystals (grains) that do not share atoms, but some HAGB are symmetric, and the grains share a certain portion of the atoms in the boundary, they are named Coincidence Site Lattice boundaries (CSL). As the name implies, the crystal lattices on either side of CSL boundaries have a degree of coincidence (Sigma – Σ). The Sigma value indicates how many atoms are shared across the boundary: Σ3 boundaries have every 3rd atom shared, Σ9 every 9th and so on. Twins are examples of CSL boundaries and the most frequent CSL boundaries in the copper materials studied here were the Σ3 and Σ9 boundaries. Σ3 boundaries (often referred to as annealing twins) show a rotation of 60.0° about the <111> axis, and Σ9 boundaries show 38.9° rotation about the <110> axis. In cubic systems Sigma boundaries are defined from Σ3 to Σ47, with the exception of low angle boundaries that are sometimes referred to as Σ1 boundaries (Rollet A D 2014, personal communication). In the Appendix all CSL boundaries and their fractions are tabled for the 9 data sets. The fraction of CSL boundaries (of total amount high angle boundaries) was calculated using the Brandon criteria (Brandon 1966, Azzi and Szpunar 2008) and 10° was used as threshold for high angle boundaries. High angle grain boundaries are indicated by black lines in Figure 1-2a,b, in this case specified as disorientations larger than 10°. Low angle boundaries are indicated by thin black lines using 2° threshold. In this case with a mainly recrystallised microstructure low angle boundaries were very few. In b) CSL boundaries are coloured in specific colours, and it is obvious that the Σ3 twins dominate the number of grain boundaries in the microstructure. > 50 % of the HAGB´s were Σ3 boundaries in all analysed positions and directions in this study. The material was from a top-sealing lid and the section was in the axial direction. Figure 1-3a shows the disorientation distribution in the same material. Disorientation defines the smallest possible rotation angle between two adjacent measurements (among the set of possible rotation solutions – often referred to as misorientations). In cubic materials the largest possible disorientation is 63°. The threshold for LAGB was set to 2° in this graph. Maxima can be seen at (1) low angles, i.e. dislocation boundaries, at (2) 40° (Σ9) and (3) 60° (Σ3). The peak at low angles show that this material was not completely recrystallised which is related to the forming process. The top-sealing lid was shaped in a forging process which will be described below in the section on Results. The cylinder walls in the large canister did not have a peak at low disorientations which can be seen in Figure 1-3b, which indicate that they have fully recrystallised microstructures.

Grain size – The average grain size can be evaluated from EBSD data by introducing thresholds that define low angle grain boundaries (dislocation-built boundaries), random high angle grain boundaries, and CSL boundaries. In Figure 1-4a,b the grain size distribution as evaluated from the large area data set of the top-sealing lid material in the axial direction is presented. The threshold for grains was set to 10°. In a) all HAGB were included, also CSL boundaries. In b) the Σ3 and Σ9 boundaries were excluded from the analysis which made the grain size very much larger. A limit for minimum size was set for a small grain to be included, in this case 10 pixels were used. The step size was 5 µm.

Crystallographic phase – EBSD is SEM based technique which is able to distinguish between crystallographic phases and crystallographic orientations, it is a very important tool for materials research and development. The high speed of modern EBSD systems makes the technique the most powerful technique for characterisation of microstructures in crystalline materials, e.g. metals.

Crystallographic texture – Crystallographic texture describes the inhomogeneous distribution of crystallographic orientations in a material. A material without texture is a material with random distribution of crystal orientations. Cast cubic metal alloys with homogeneous nucleation often show random distributions of crystal orientations (in this case equal to a random distribution of grain orientations). Crystallographic texture in metallic construction materials is developed during the thermo-mechanical processing, e.g., hot rolling, cold rolling, forging, extrusion and sheet metal forming processes as a result of crystal rotations. The 3-dimensional distribution of orientations are often described as a distribution in "Euler space" (Van Houtte 1987) and can be plotted using the "Orientation distribution function" (ODF) (Bunge 1992). The 3-dimensional information can then be analysed in 2-dimensional sections of the 3-dimensional ODF. The orientation distribution is also often given in "Pole figures" or "Inverse pole figures" where the 3-dimensional information is projected to a 2-dimensional plane which makes the information easier to understand. Texture strength can be calculated for the ODF as well as for pole figures and give information on how inhomogeneous the orientation distribution is in terms of multiples of the random distribution. It is important to analyse a representative area large enough to give a correct description of the material when texture is analysed. Too small an area, or an area with too few grains, will give incorrect information. As a rule of thumb more than 1 000 grains should be included in a texture analysis. In this work texture strength was determined by a commercial software from Oxford Instruments, "AZTEC Crystal". The texture was calculated using serial expansion mathematics and more information on this can be found in textbooks on textures in metals, e.g. (Bunge 1992).

Corrosion aspects on metallic materials can often be connected to the microstructure, for example the phase distribution in multiphase materials, precipitation of particles in a grain boundary which drains the surrounding matrix of alloying elements, inter-metallic phases and inclusions. All these features can play an important role for corrosion properties. It is also reported that the different crystallographic planes have different corrosion properties. The difference is not dramatic but Lindell (Lindell and Pettersson 2015) reports a factor of two in mean corrosion rate in austenitic stain-less steel between the most corrosive planes (<100>) compared to the least corrosive (<111>). With data available from EBSD analysis it is possible to analyse which planes that are parallel to the surface and thus exposed for corrosion attack.

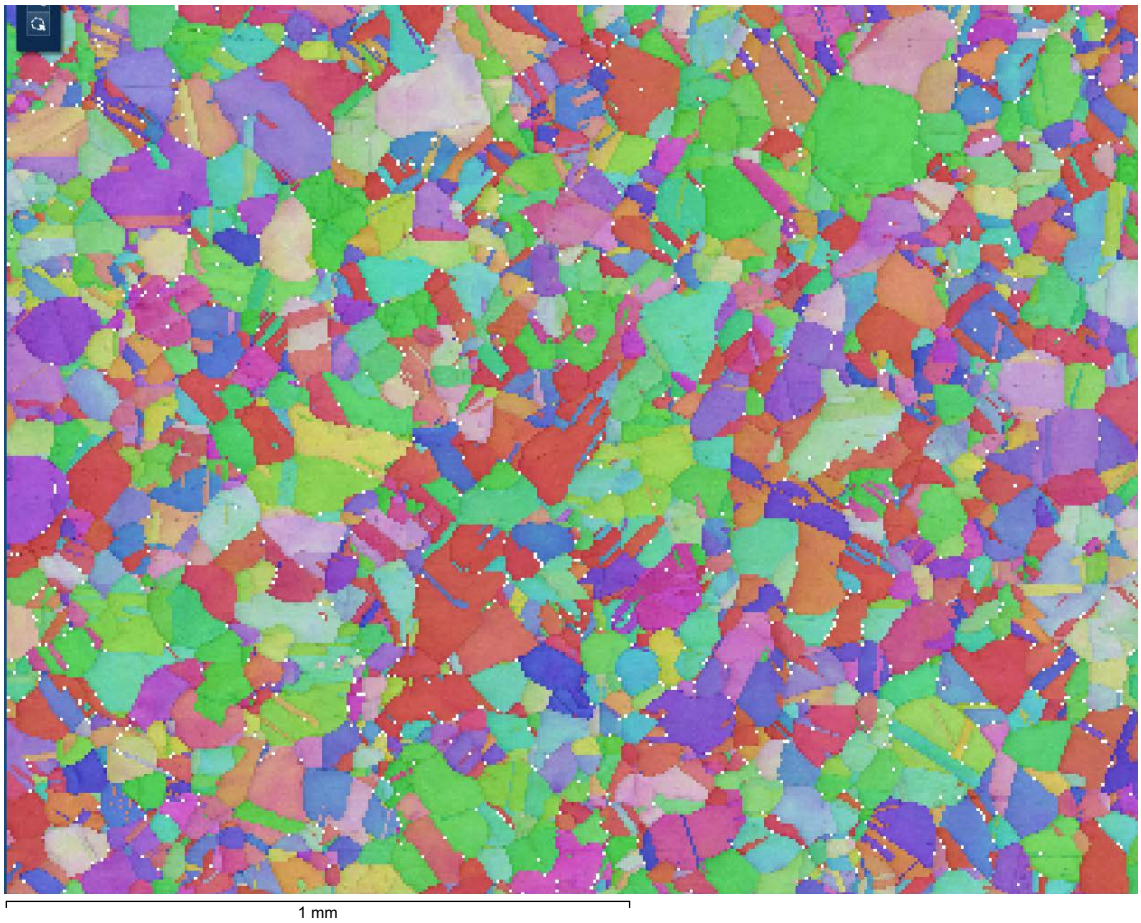

Figure 1-1. *An example on EBSD raw data with non-indexed pixels (white). The cleaning uses the surrounding pixels to give the non-indexed pixel an Euler angle value.*

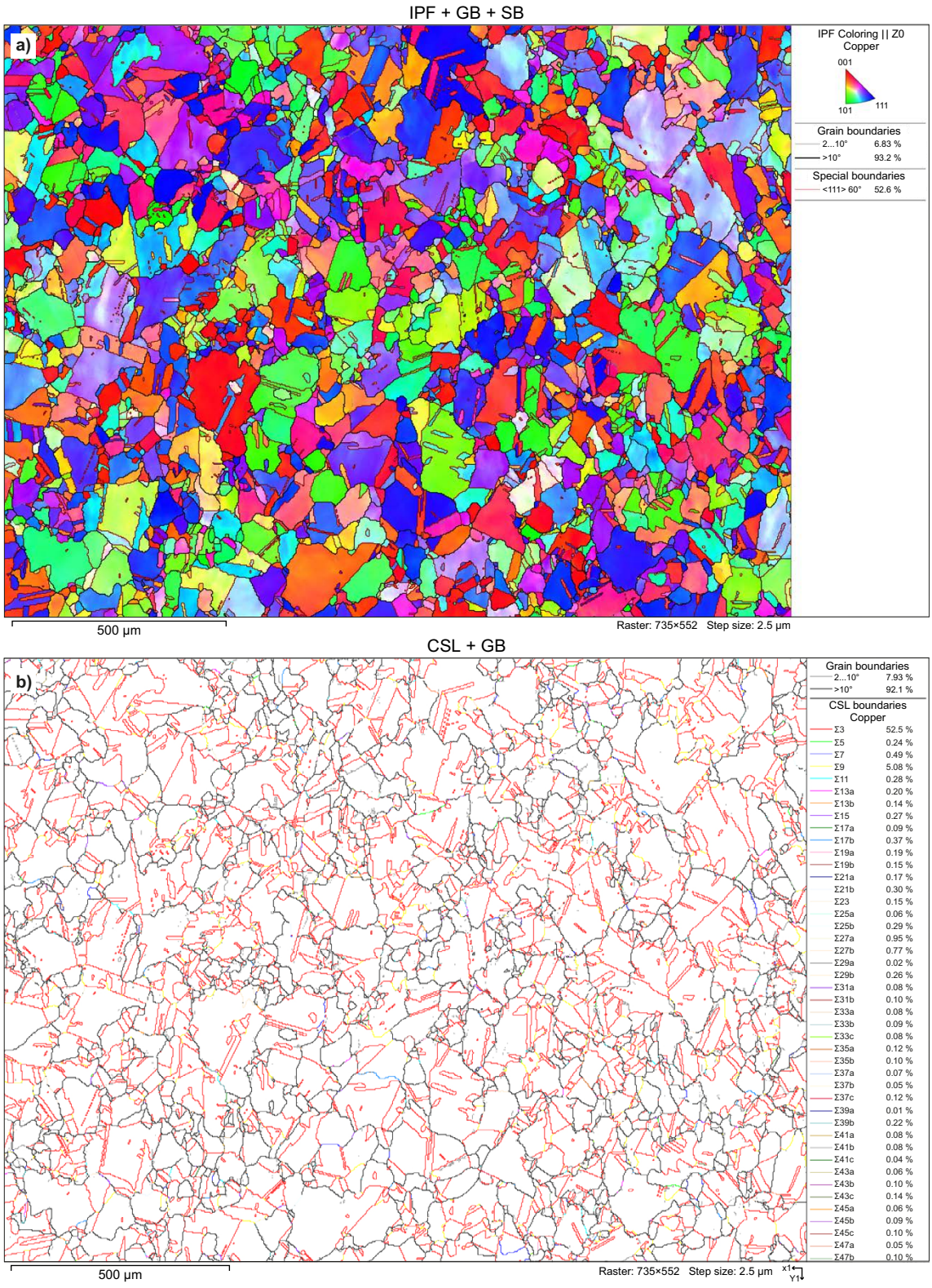

Figure 1-2. *EBSD data from one single EBSD map (from top-sealing lid) plotted in two ways. The analysis used 2.5 µm step size and was built up from 735 × 552 individual point analyses. a) Crystallographic orientations plotted using colours according to the inverse pole figure (IPF). b) CSL grain boundaries.*

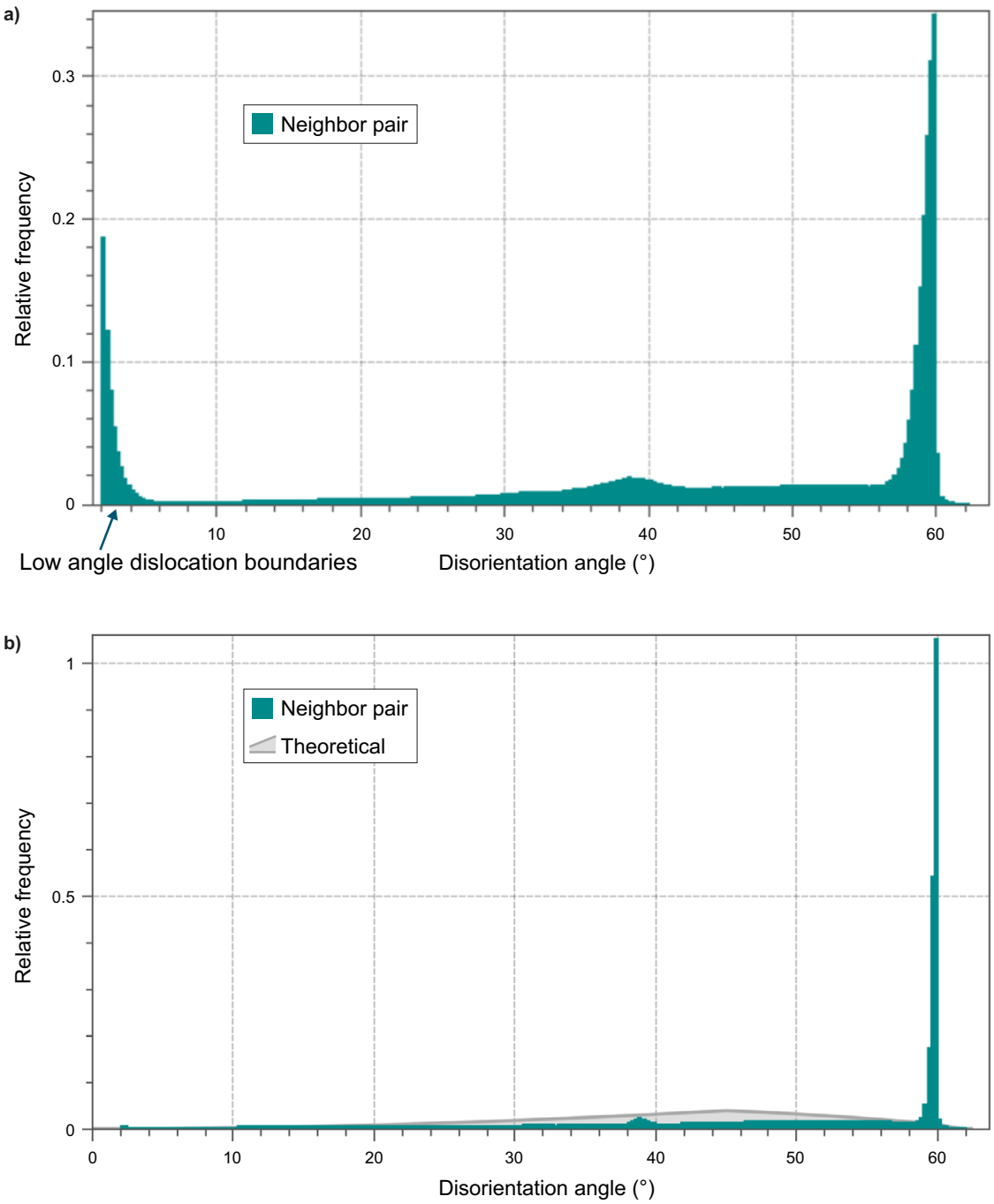

Figure 1-3. *Disorientation distribution in the top-sealing lid (a) and the canister wall (b). The threshold for LAGB was set to 2°. In the lid material maxima can be seen at low angles (Σ1, dislocation boundaries), at 39° (Σ9) and 60° (Σ3). In the canister wall which was fully recrystallised the peak at low angles is missing.*

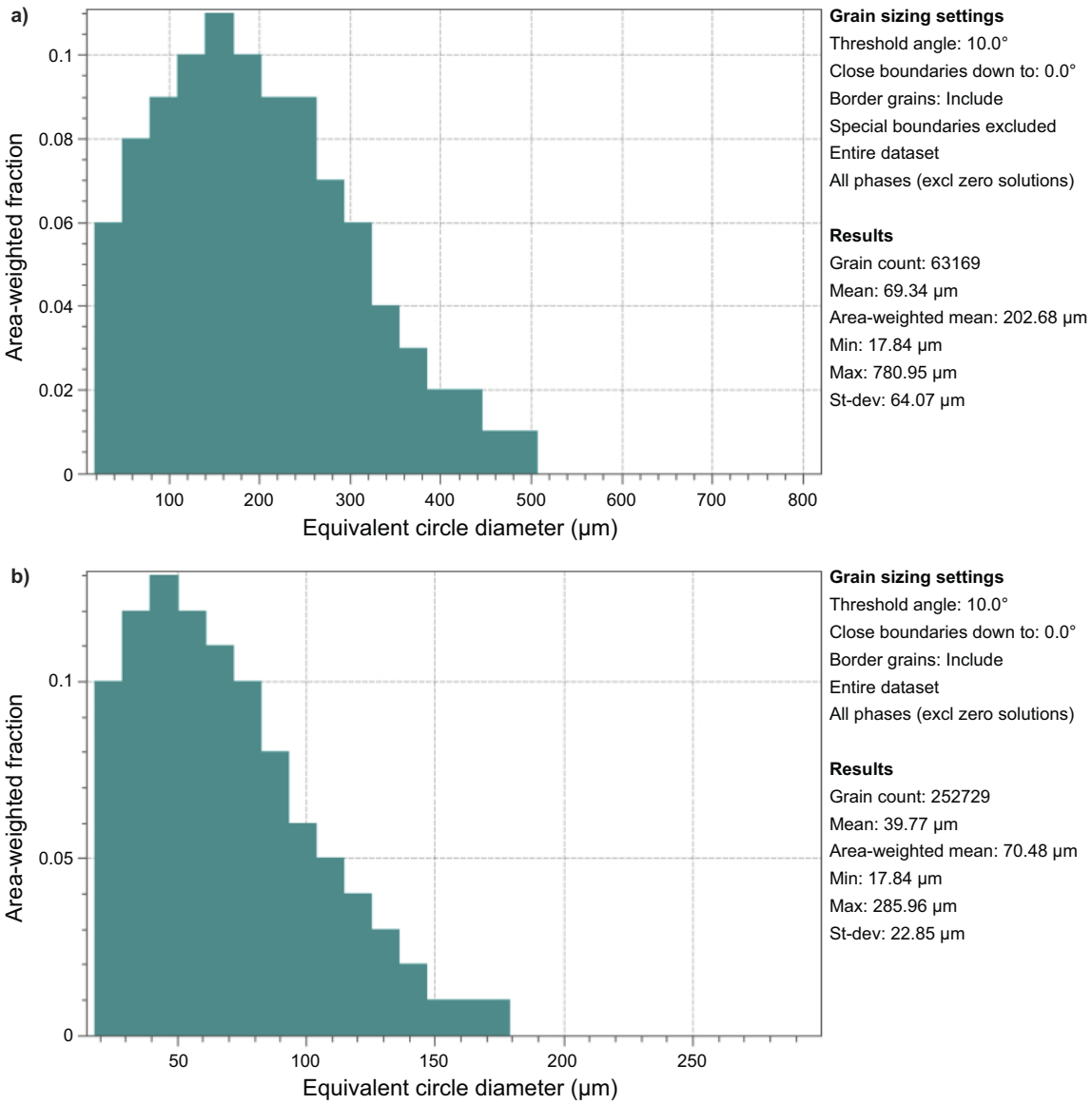

Figure 1-4. *Grain size distribution. This data is from a large area map from the top-sealing lid material in axial direction. If special boundaries were excluded the number of grains were 63 169 and the average diameter was 202 µm. When CSL boundaries were included the number of grains were instead 252 729 and the average diameter was 70 µm. The graph shows area weighted grain size which is not the same as arithmetic grain size.*

2 Materials

The copper material in this study was taken from the walls of two different cylindrical canisters and one canister lid. Ten specimens from different positions and directions were chosen to get detailed information on the materials microstructure and any inhomogeneity. Specimens for analysis in different directions in the wall (radial, tangential or axial) were fabricated. The radial direction is equivalent to the thickness direction in the canister wall. Table 2-1 and Figure 2-1 give details about the specimens. The canisters were analysed using ultrasonic sound before this work and "Fine" and "Coarse" microstructures were identified (information from SKB). The column labelled "structure" in Table 2-1 refers to this analysis. The term "Position in thickness direction" simply defines the depth below the surface that the analyses were done. For example, "Through thickness" refers to an analysed surface which spans the entire thickness of the wall in the radial direction, whereas "Half" refers to a surface parallel to the canister surface at mid thickness. Two specimens were cut from a top-sealing lid part that was stored at Swerim, TX219. One specimen in the axial direction and one in the tangential direction. Both were taken from the outer rim of the piece stored at Swerim. Then three specimens were cut from the cylinder wall from a part with ID "T77". One specimen in axial direction with fine microstructure, one specimen in tangential direction with coarse microstructure and one in radial direction also with coarse microstructure. Additionally, five specimens were cut from the cylinder wall from a part with ID "T101". One in axial direction with coarse microstructure and one with fine microstructure, one in tangential direction with fine microstructure, and then two specimens in radial direction were cut to represent the cylinder surface and the mid thickness. The directions are referred to the normal direction of the surface for analysis. The directions in the cylinder are explained in Figure 2-1. The lid material was defined with the same directions as the canister, the lid surface normal direction is therefore equal to the (cylinder) axial direction (and this is also the thickness direction in the lid).

Specimens were cuboids with a base of 50 × 30 mm and 20 mm height. Specimens from the canister wall in the tangential and axial directions were cut through the wall thickness enabling analysis of differences in microstructure in the thickness direction.

The cutting was done using wire EDM, Electrical discharge machining, also known as spark machining, spark eroding, die sinking, wire burning or wire erosion. EDM is a metal fabrication process whereby a desired shape is obtained by using electrical discharges (sparks). Material is removed from the work piece by a series of rapidly recurring current discharges between two electrodes, separated by a dielectric liquid and subject to an electric voltage. The cutting is made under water and the material is not heated. Further grinding and polishing steps are explained under "Experimental".

Table 2-1. Description of specimen positions and prepared surfaces normal directions. The structure was analysed with ultrasonics prior to EBSD, and the microstructure was characterised as fine or coarse. The mapped sections were 50 mm × 15 mm. When "through thickness" then the entire wall thickness was analysed from the outer to the inner surface.

Nr	Part	Direction	Structure	ID	Position in thickness direction
1a	Tube	Axial	Fine	T77	Through thickness
1b	Tube	Axial	Fine	T101	Through thickness
2	Tube	Axial	Coarse	T101	Through thickness
3	Tube	Tangential	Fine	T101	Through thickness
4	Tube	Tangential	Coarse	T77	Through thickness
5	Tube	Radial	Fine	T101	Outer surface
6	Tube	Radial	Coarse	T77	Half
7	Tube	Radial	Fine	T101	Half
8	Lid	Axial	Coarse	TX219	Half
9	Lid	Tangential	Coarse	TX219	Through thickness

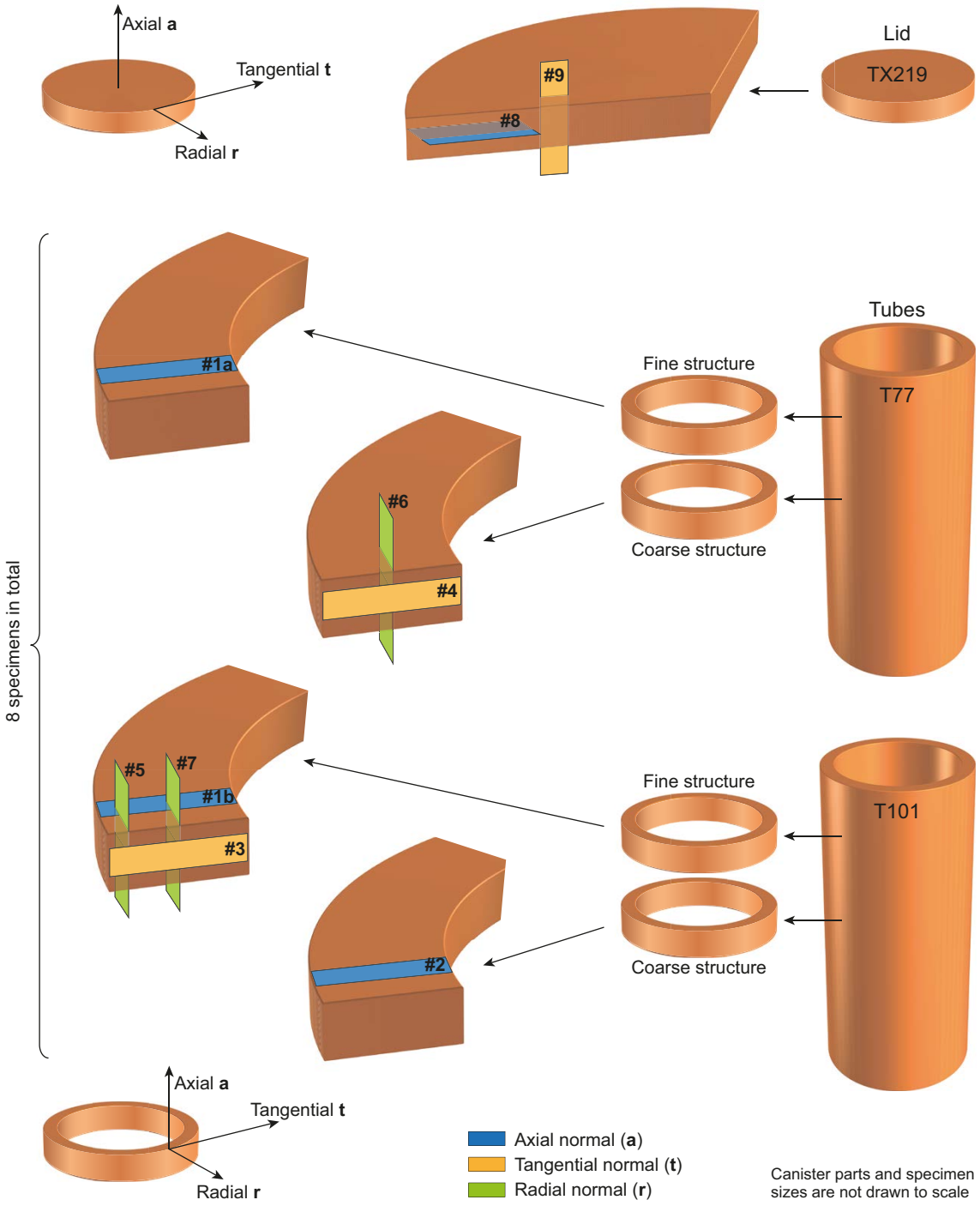

Figure 2-1. *Specimen directions in the canister wall and lid. The directions are referred to as the normal direction of the surface for analysis. Thickness direction in the tube wall is synonymous to radial direction, while thickness in the lid is in axial direction.*

3 Experimental

The specimens were prepared for metallographic analysis in SEM/EBSD. EBSD is a SEM based technique with high spatial resolution as described in the introduction. The penetration depth for EBSD analysis is very small, the diffraction is induced from 2 to 5 nm depth below the surface. It is therefore very important to prepare the surface such that it is not damaged by plastic deformation by e.g. remains from grinding or diamonds scratching the surface during polishing. EDM was used to cut the specimens from the large canister to minimize the damage from cutting (described above under "Materials"). Next step was grinding using SiC paper, starting with P320 and finishing with P4000. Diamond polishing was then executed in 4 steps with 6 µm, 3 µm, 1 µm and 0.25 µm diamonds. For large specimens like this it is difficult to get the complete surface perfectly polished by conventional methods and the final step to obtain a completely damage-free surface was in this case a combination of electro-polishing and oxide particle suspension (OP-S). Electro-polishing was performed using orthophosphoric acid and water (50/50), electro-polishing effectively removes material leaving deformation free surfaces, however etching was a problem and to get around this problem OP-S polishing was added. This extra preparation step using OP-S with additions of ammonia and hydrogen peroxide (90 ml OP-S, 6 ml ammonia and 4 ml hydrogen peroxide) successfully improved the surface and the final surface condition showed to be perfect for EBSD.

The EBSD analyses were made using a Zeiss GeminiSEM450 microscope. This microscope can deliver high current combined with a small spot which is important for high speed EBSD analysis. The EBSD detector was an Oxford instrument Symmetry detector which can be run at very high speed, > 3 000 Hz, but often lower speeds are chosen for improved pattern quality. In this case very large areas were analysed by combining many individual EBSD maps that automatically were stitched together, typically the analysed area was 45–48 mm versus 12–15 mm. The step size was 5 µm which resulted in data sets of about 25–30 million points. Running at 2 000 Hz one specimen took typically 6 hours effective analysis time in the microscope. Set-up and optimisation etc added an extra hour. Analyses, post-processing to extract specific information, of the data was instead the most time-consuming part of the work.

When acquiring EBSD data commonly not every single point can be indexed, this is due to surface imperfections (dirt, scratches, residuals from preparation, dust, …), particles or secondary phases and defects in the crystal structure (grain boundaries, pores, cracks, …). In this case it was mostly pixels in grain boundaries that were not indexed. The overall fraction of non-indexed points was low, < 2 %, and it was therefore safe to remove these pixels by a "cleaning" process. The AZTEC Crystal software (Oxford instruments) contains methods to this is in a controlled way.

4 Results

4.1 Overview

Analyses were made for 10 specimens, 2 specimens from the top-sealing lid, 3 specimens from canister T77 tube wall and 5 specimens from canister T101 tube wall. The analysed surfaces normal directions are explained in Figure 2-1. The directions are defined in reference to the long axis of the cylindrical canister. Detailed results with images and graphs, and description of data and procedures for analysing the data are given below for each specimen.

EBSD analysis in the SEM is made on a 70° tilted sample and the accuracy of the grain size determination is dependent on the geometry of the specimen and microscope set-up. If the surface is not perfectly flat, and if the specimen and stage geometries are not perfectly aligned then the surface dimensions will not be correct and as a consequence the grain size determination will be affected. In the ISO standard for grain size analysis using EBSD this is discussed and Mingard et al. (2012) performed round robin exercises to evaluate the error between labs (Mingard et al. 2012, ISO 2020). Furthermore, the SEM need to be well calibrated. In this case all the specimens were prepared by EDM cutting in a high precision instrument and grinding and polishing were carried out with special attention to keep the specimen geometry perfectly aligned. The SEM was calibrated by service engineers from Zeiss. These geometry related issues mainly concern grain size analysis and absolute crystal orientation in reference to the specimen directions. For grain boundary character determination it is the relative orientation between two adjacent measurements (pixels) that defines the grain boundary disorientation. The error between adjacent measurements is very small, below 0.5° for normal high speed analysis and below 0.05° for slower analysis using higher resolution patterns (Thomsen et al. 2013). In this case the normal high speed conditions were applied but the error in the analysed grain boundary disorientation distribution must in any case be considered to be very small. The analysis of CSL boundary fractions is based on these data and the error in these analyses are small. The analysed area of each specimen was > 500 mm^2 and the number of analysed grains was > 50.000 in each specimen.

Table 4-1 presents summarized results from the analysis of CSL boundary fraction. The results show that the Σ3 twin boundary was very common in the canister copper material, about 50 % of the high angle boundaries in the material was of Σ3 twin character. The variation with specimen orientation in the tube wall was small, 50.5 ± 0.7 %, but one position and direction showed significantly higher fraction of Σ3 twin boundaries; the tube material in radial direction close to the canister surface (53.7 %). Position 5 was from the same material but mid thickness in the tube wall and did not show similarly high fraction. Another significant difference was that the number of Σ1 and Σ9 boundaries were higher in the lid, this is connected to the deformed microstructure in the lid.

The fraction low angle grain boundaries (LAGB) was very different in the canister walls and lid, the lid that was not fully recrystallised contained substantial instances of dislocation-built LAGB, around 24 %, but the walls contained only low amounts, around 3 %. Close to the canister wall outer surface the amount of LAGB was higher compared to the average over the wall thickness, around 5 %.

Grain sizes are presented in Table 4-2 and texture strength in Table 4-3. The grain size in the tube material did not vary a lot, the arithmetic mean diameter was 64.3 – 69.0 µm in the specimens that were attributed as fine and 65.6 – 71.1 in the specimens attributed as coarse. The area weighted mean showed larger variance as can be seen in Table 4-2. The lid material showed significantly larger grain size compared to the canister wall material. The difference was not very big for the arithmetic mean diameter, but the area weighted mean and the largest grains were both clearly larger.

Texture strength as evaluated from pole figures showed similar value for the specimens in the canister wall, around 5 times random. The lid showed weaker texture strength, around 2 times random.

Table 4-1. Results from the analysis of CSL boundaries, fraction (%).

CSL boundary	1a. T77 Axial F	1b. T101 Axial F	2. T101 Axial C	3. T101 Tang F	4. T77 Tang C	5. T101 Radial F	6. T77 Radial C	7. T101 Radial F	8. Lid Axial C	9. Lid Tang C
Σ1 (LAGB 2–10°)	2.85	2.68	2.96	2.59	2.50	2.90	2.42	4.63	17.0	24.4
Σ3 60.00° <111>	49.78	50.64	51.13	49.86	49.98	51.18	50.20	53.71	51.96	48.53
Σ5 36.87° <100>	0.22	0.21	0.21	0.21	0.22	0.22	0.24	0.20	0.32	0.32
Σ7 38.21° <111>	0.64	0.64	0.64	0.64	0.63	0.63	0.64	0.57	0.45	0.51
Σ9 38.94° <110>	2.59	2.34	2.26	2.33	2.53	2.44	2.64	2.16	5.31	5.03
Σ11 50.48° <110>	0.54	0.53	0.52	0.55	0.55	0.53	0.53	0.56	0.48	0.52
Σ13a 22.62° <100>	0.16	0.15	0.15	0.15	0.15	0.14	0.16	0.14	0.14	0.15
Σ13b 27.8° <111>	0.27	0.27	0.26	0.27	0.28	0.27	0.28	0.26	0.21	0.25
Σ13c 49.22° <322>	0.86	0.83	0.84	-	0.85	-	-	-	-	0.80
Σ15 48.19° <210>	0.31	0.30	0.29	0.31	0.31	0.30	0.32	0.27	0.33	0.34
Σ17a 28.07° <100>	0.07	0.07	0.06	0.07	0.07	0.07	0.07	0.07	0.08	0.08
Σ17b 61.93° <221>	0.38	0.38	0.39	0.38	0.38	0.38	0.37	0.37	0.30	0.32
Σ19a 26.53° <110>	0.20	0.20	0.20	0.20	0.20	0.20	0.21	0.20	0.26	0.28
Σ19b 46.83° <111>	0.17	0.17	0.17	0.17	0.16	0.17	0.16	0.15	0.12	0.14
Σ21a 21.79° <111>	0.17	0.18	0.17	0.18	0.18	0.18	0.17	0.16	0.13	0.15
Σ21b 44.4° <211>	0.26	0.25	0.25	0.24	0.26	0.25	0.26	0.24	0.25	0.26
Σ23 40.45° <311>	0.14	0.14	0.13	0.14	0.14	0.14	0.15	0.13	0.18	0.18
Σ25a 16.25° <100>	0.11	0.11	0.10	0.11	0.11	0.10	0.10	0.10	0.08	0.10
Σ25b 51.68° <331>	0.38	0.37	0.35	0.37	0.36	0.36	0.36	0.35	0.31	0.34
Σ27a 31.58° <110>	0.44	0.40	0.39	0.40	0.45	0.41	0.45	0.32	0.85	0.80
Σ27b 35.42° <210>	0.30	0.26	0.25	0.27	0.30	0.27	0.31	0.19	0.79	0.76

F = Fine microstructure, C = Coarse microstructure (measured with ultrasonic sound).

Table 4-2. Average and maximum grain size.

Grain size diameter (µm)	1a. T77 Axial F	1b. T101 Axial F	2. T101 Axial C	3. T101 Tang F	4. T77 Tang C	5. T101 Radial F	6. T77 Radial C	7. T101 Radial F	8. Lid Axial C	9. Lid Tang C
Arithmetic mean	65.8	69.0	71.1	69.0	65.8	68.9	68.1	64.3	69.4	67.4
Area weighted mean	123.9	131.1	135.7	130.6	124.4	130.1	139.2	118.8	201.5	203.0
Maximum	465	459	494	499	617	467	493	533	798	725

Table 4-3. Texture strength in pole figures.

Texture strength	1a. T77 Axial F	1b. T101 Axial F	2. T101 Axial C	3. T101 Tang F	4. T77 Tang C	5. T101 Radial F	6. T77 Radial C	7. T101 Radial F	8. Lid Axial C	9. Lid Tang C
Times random	5.5	5.3	5.3	5.6	5.5	4.8	4.5	4.6	1.6	2.0

4.2 Top-sealing lid material

4.2.1 Lid axial direction – analysed surface normal was parallel to the axial direction. Fine microstructure (specimen #8, Table 4-2)

The analysed surface was parallel to the lid surface, with X along the radial direction and Y along the tangential direction. The surface was from mid-thickness in the wall. Figure 4-1a,b shows the crystallographic orientations in the large-area stitched EBSD map with two different reference axes. The analysed area was 41 mm (X) and 10 mm (Y). The step between each analysed pixel was 5 µm. In these figures crystallographic orientations were plotted using the inverse pole-figure colour key (IPF) (shown in Figure 4-1c). In a) the reference direction was Z which is equal to the axial direction and in b) the reference direction was Y (equal to radial direction). The difference that can be seen in colours between the two directions indicates that the crystallographic orientations were not randomly oriented in the material, i.e. a crystallographic texture is present in the material. The origin of texture is often from the thermo-mechanical processing which in this case included rolling and as the final step a forging operation. In the IPF Z EBSD crystallographic map (a) red and blue colours were dominating and from the IPF colour key (c) it can be learned that red represents <100> planes parallel to the analysed surface and blue represents <111> planes. In the IPF Y map (b) green is more frequent which represents the <110> planes. Figure 4-2 shows the pole figures plotted with the acquisition axes as X, Y and Z, where Z is the axial direction, X is the radial- and Y is the tangential direction. Since the lid was produced from a forged plate Z is also the normal direction in the plate.

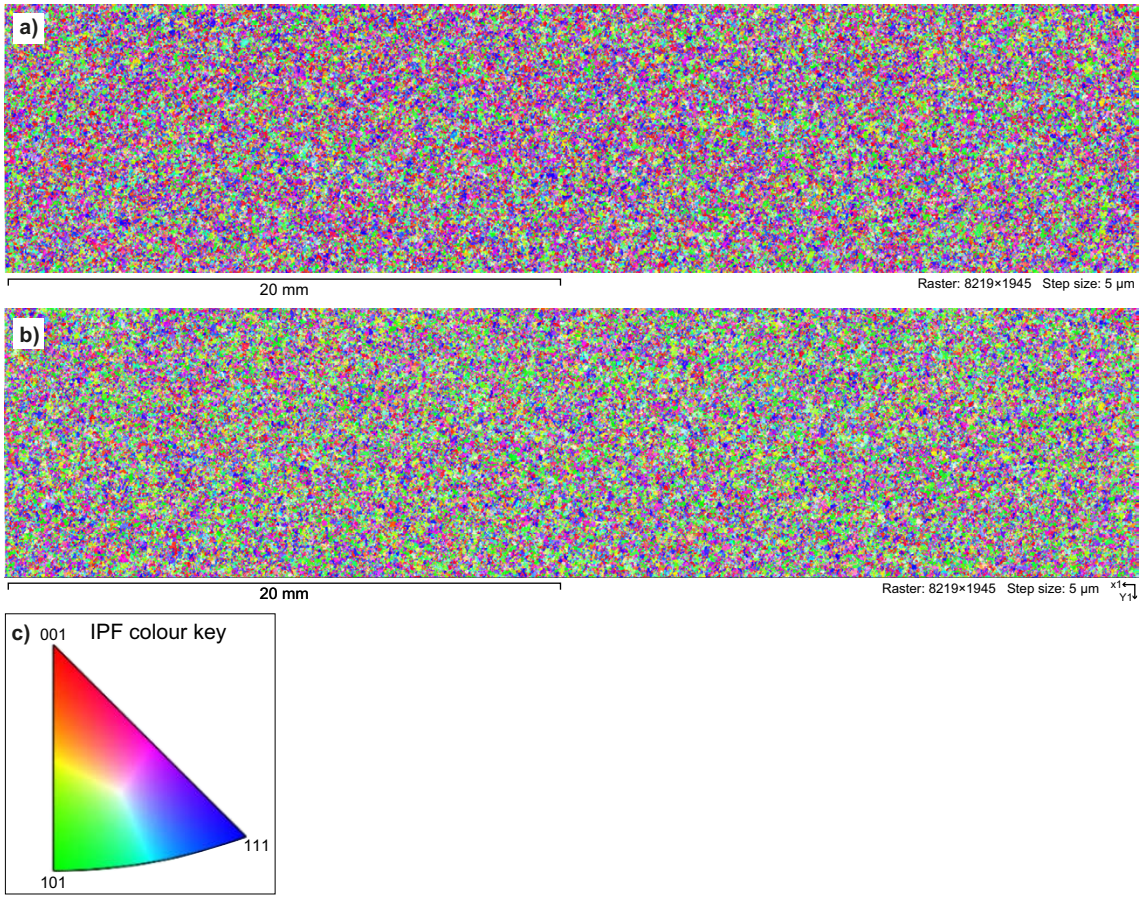

Figure 4-1. *EBSD crystal orientation map analysed on a surface parallel to the lid surface. The analysed plane normal was parallel to the canister axial direction (the lid thickness direction). The analysed area was 41 mm (X) and 10 mm (Y). The step between each analysed pixel was 5 µm giving 15.8 million pixels. In a) colours show orientations with reference to the axial direction (Z) and in b) in the radial direction (Y). In c) the key to the colours are given.*

Figure 4-2 shows the pole figures from close to 16 million data points. The texture was weak in this analysed section, 1.6 times random (half width 5°), but the maxima in the centre of the <100> pole was distinct and shows that there is a preferred direction in the normal (Z) direction. The maxima in the <110> and <111> were rotated from the radial/tangential reference and not aligned in X (radial) or Y (tangential). The specimen was 45 mm wide and taken from the round lid. The rolling direction in the rolling of the plate that was forged was not known and it is probable that the origin of the texture was from rolling, and not from the forging. This explains the asymmetry in the pole figures which appear to be rotated. Only the axial direction remains the same since the normal direction of the plate was the same in hot rolling and forging.

The grain size analysis from the large area analysis is presented in Figure 4-3. The analysis identified > 63 000 grains which gave a lot of statistics. The threshold for grains was set to 10 pixels in accordance with the ISO standard (ISO 2020), and with a step size during analysis of 5 µm the smallest accepted grain was 18 µm. The threshold for disorientation to be a grain boundary was set to ≥ 10°. The most common twin boundaries, Σ3 and Σ9 were excluded from the analysis. Figure 4-3 shows the area weighted grain size. The arithmetic mean diameter was 69 µm, the area weighted mean 202 µm and the largest grain was 798 µm.

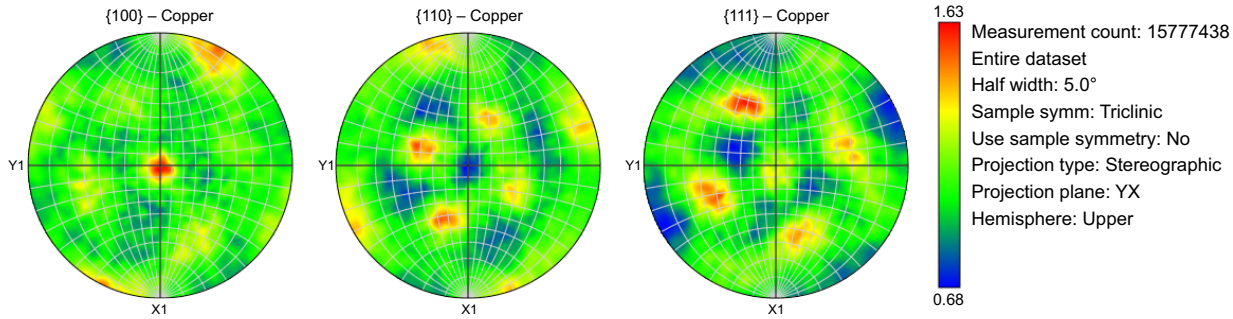

Figure 4-2. *Pole figures in the normal direction of the canister lid. The data set is from the complete analysis and contained almost 16 million measurements.*

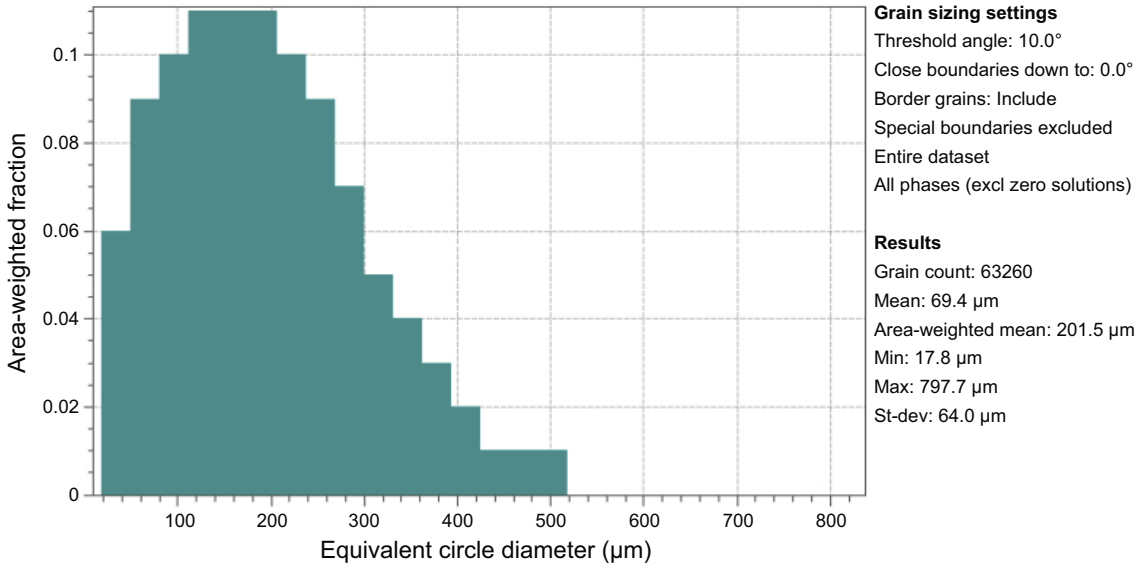

Figure 4-3. *Grain size distribution in the top sealing lid material measured in the axial direction (i.e. the normal direction of the analysed area parallel to the canister axial direction) The axial direction was also the thickness direction in the lid. 63 260 grains were included in the analysis.*

The grain boundary disorientation distribution for the top-sealing material measured in the axial direction is shown in Figure 4-4. The peak at low angles indicates that the material was deformed after recrystallisation. The peaks at 60° and 39° are from the Σ3 and Σ9 twin boundaries.

The analysis of CSL boundaries was based on the Brandon criteria (Hagström et al. 2015, Trimby 2009). For the analysis of the fraction of HAGB that were CSL type boundaries 10° was used as the threshold for a grain boundary to be regarded as a high angle grain boundary (HAGB). Grain boundaries with lower disorientation were regarded as dislocation-based boundaries. The fractions are labelled in the Appendix. In this data set from the top-sealing lid and a section in the axial direction 52 % of the HAGB were Σ3 and 5.4 % Σ9.

To explore variations in the microstructure in the large analysed area the data set was divided into 9 smaller datasets according to Figure 4-5. Each data set was then analysed individually to get the grain size and texture. The results showed very small differences in this case. This specimen, top-sealing lid in the axial direction, was not expected to vary a lot since the whole area was from the same depth in the lid thickness direction and the whole area was at about the same distance from the lid centre. Larger variations are expected from specimens taken out from the cylinder wall, through the wall thickness.

With data available from EBSD analysis it is possible to analyse which planes that are parallel to the surface. This information is interesting in understanding corrosion rates since there is a relationship between crystal planes and corrosion rate. Figure 4-6 plots the three most common close-packed planes that are parallel to the top surface of the lid. It is possible to get the fractions of any crystallographic plane, in this case red is <100>, green is <110> and blue is <111>. The fractions were calculated with a 15° spread from the ideal orientation. The result of the analysis was that <110> planes were most frequent with a fraction of 16.4 %, then <111> planes were second most frequent (15.9 %) and <100> planes the least frequent ones (13.9 %). The texture is weak in the material and therefore also the difference in occurrence between close packed planes is small.

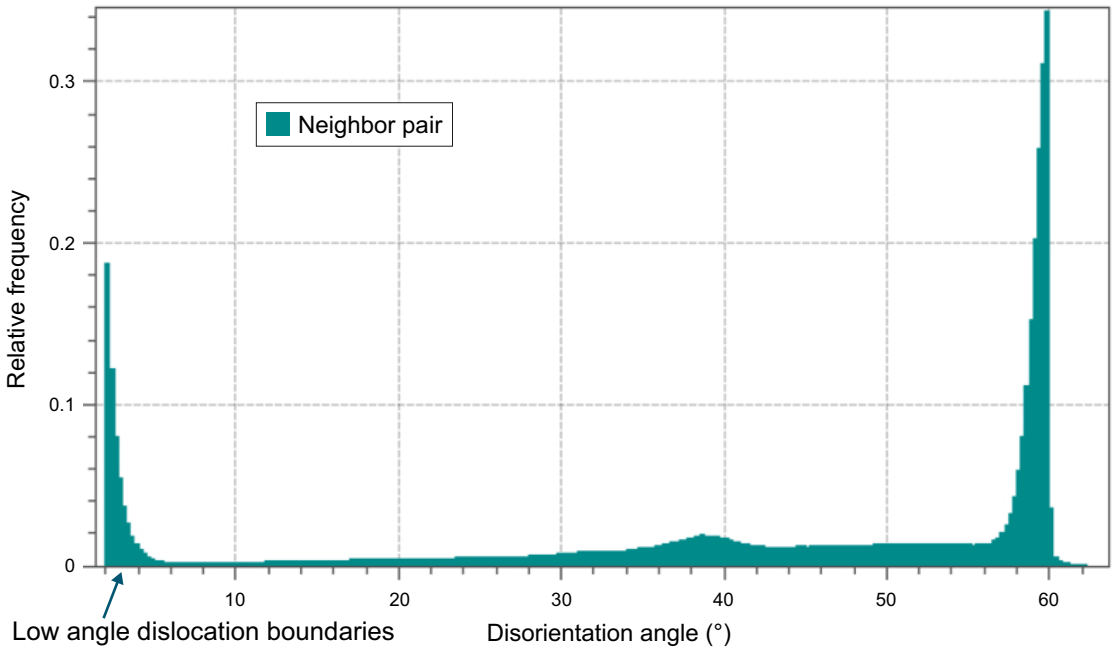

Figure 4-4. *Grain boundary disorientation distribution for the top-sealing material. The peak at low disorientation was due to dislocation boundaries and indicates plastic deformation in the microstructure. The peaks at 60° and 39° were due to the Σ3 and Σ9 twin boundaries.*

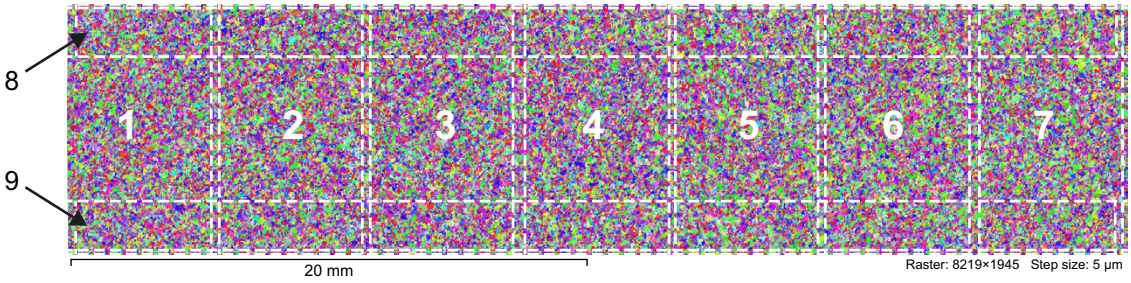

Figure 4-5. *Division in small sub-sets to explore the variation of grain size and texture over the section.*

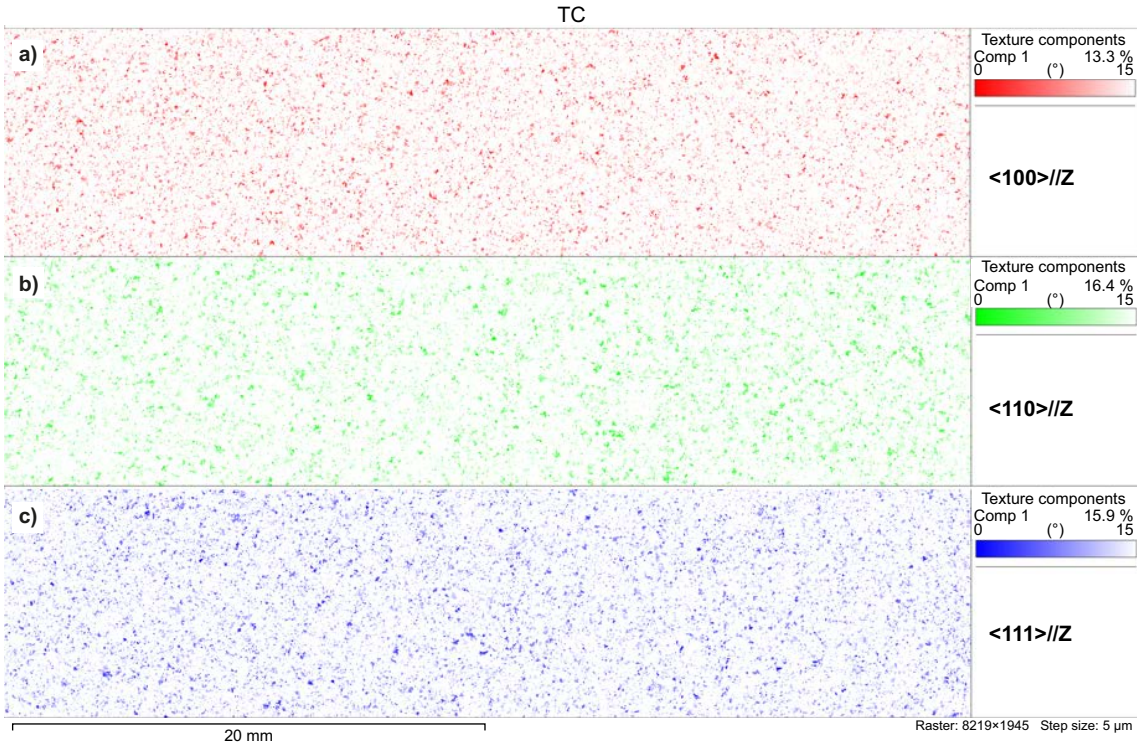

Figure 4-6. *Fractions of close-packed planes parallel to the surface of the lid.*

4.2.2 Lid tangential direction – analysed surface normal was parallel to the tangential direction. Coarse microstructure (specimen #9, Table 4-2)

The crystallographic orientations in the tangential section are shown in Figure 4-7a,b. The colours represent orientations with reference to IPF in the axial direction and tangential direction. This section spans the distance from the bottom surface to the top surface of the lid and it could be expected to contain more differences in the microstructure compared to the section for specimen #8 in axial direction. It is a visual shift in colour from the top (left side) to the bottom (right side) which indicate a change in texture from more <100> (red) to more <110> (green). Figure 4-7c shows the pole figures plotted with the acquisition axes as Y, Z and X, where X is equal to the canister axial direction (lid thickness direction), Y is the radial and Z is the tangential direction. Since the lid was a forged plate, X is also the normal direction in the plate. The texture was weak, 2.0 times random (half width 5°). The maxima in the centre of the <100> pole was distinct and shows the preferred direction in the normal (X) direction. The maxima in the <110> and <111> were in this case aligned in Y and Z. The analysed area in this section was more aligned along symmetry axes from the hot rolling compared to the axial section, which was the reason for the symmetry in the pole figures. Figure 4-7d shows the texture at the top surface of the lid. The texture changed from a well defined <100> (fibre) texture with 2.4 times random strength and a weaker <111> texture at the top surface to a weaker (1.8 times random) fibre texture with maxima in <100> and <111> at the bottom. The description of the textures as fibre textures is because the only one direction is well defined (the normal direction), the other plane directions are rotated which forms a circle in the pole figures.

The grain distribution is presented in Figure 4-8. The grain size was larger at the top surface (left) of the lid compared to the bottom surface (right), with a mean diameter of 67 µm (area weighted mean 218 µm) at the top and 66 µm (area weighted mean 190 µm) from about quarter depth and closer to the bottom surface. The mean arithmetic grain size for the whole section was 67 µm and more than 87 000 grains were included in the data set. The area weighted mean was 203 µm. Compared to the axial section (from wall mid thickness) the average grain size was similar in this section.

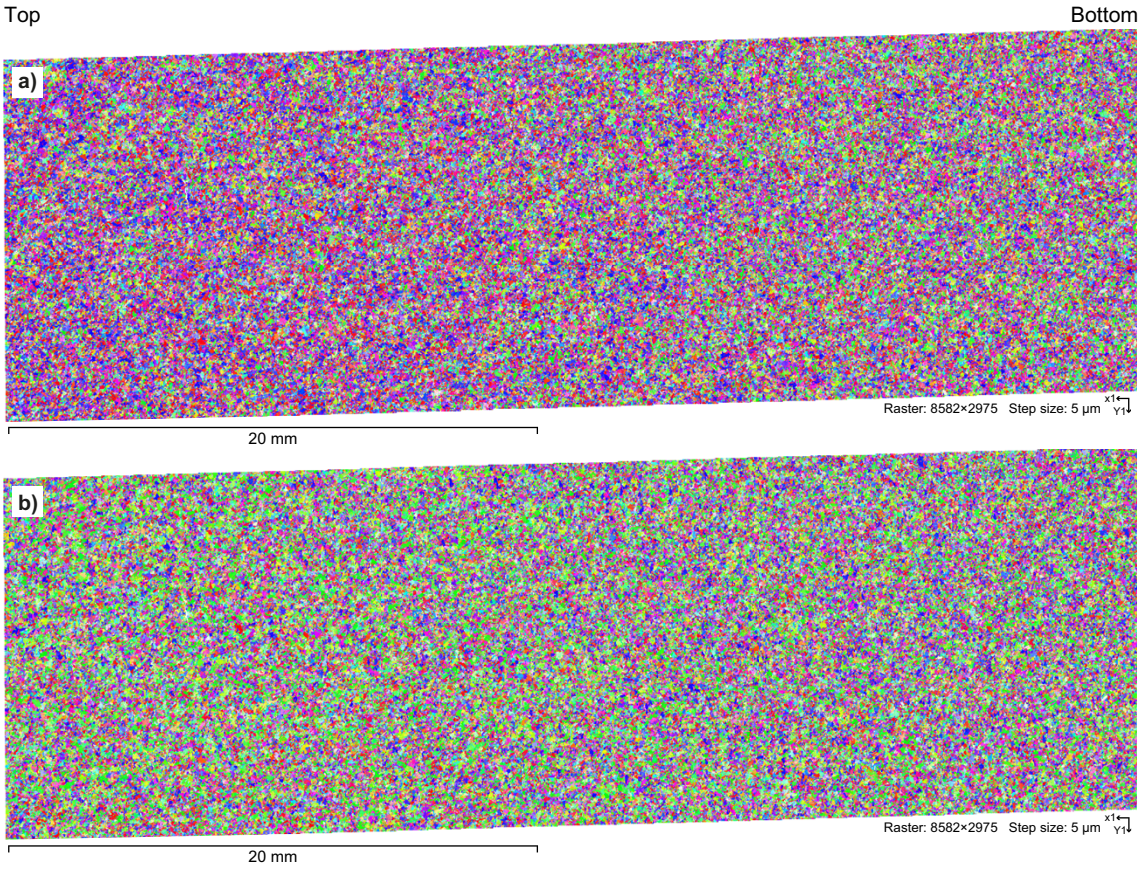

Figure 4-7a,b. *EBSD crystal orientation map analysed on a surface with the plane normal direction parallel to the tangential direction. The analysed area was 43 mm (X) and 15 mm (Y). The step between each analysed pixel was 5 µm giving 23.5 million pixels. In a) colours show orientations with reference to the axial direction and in b) in the tangential direction. The key to the colours is given in Figure 4-1c.*

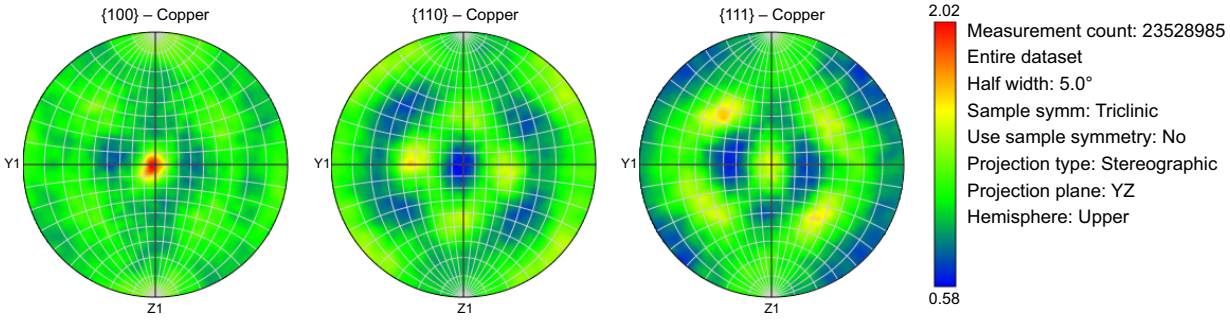

Figure 4-7c. *Pole figures from the whole data set in the lid normal direction (X).*

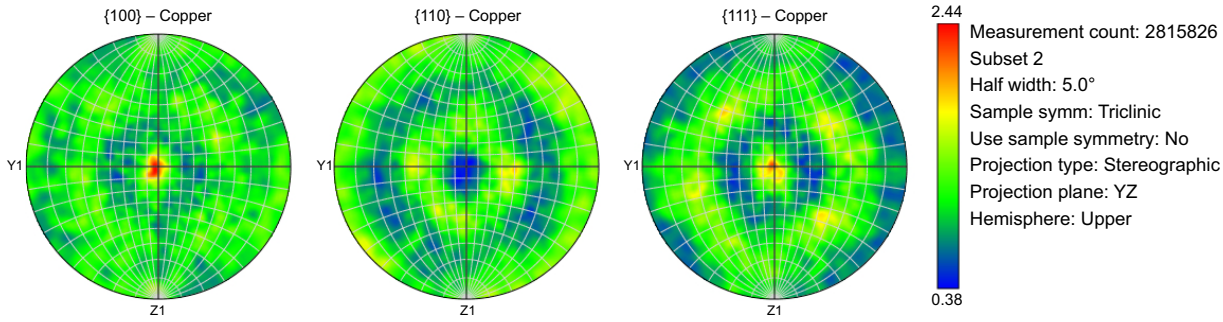

Figure 4-7d. *Pole figures from the top (left) surface data set. The rings in the pole figures show that the crystallographic close packed planes are rotated around the normal direction. The texture can be described as weak <100> and <111> fibre textures in the normal direction.*

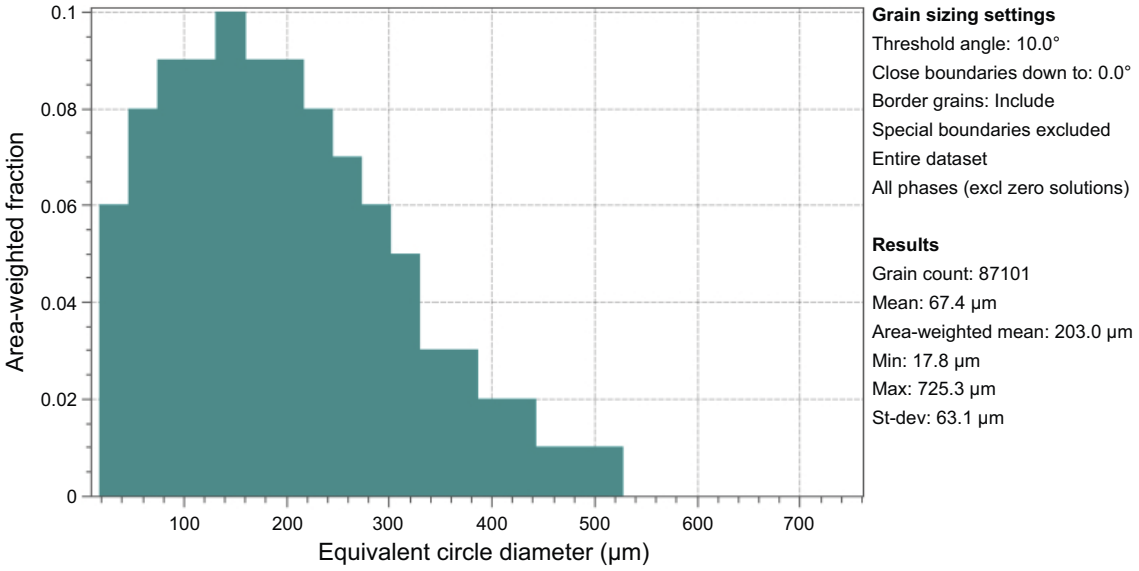

Figure 4-8. *Grain size analysis from the whole data set with 87 101 grains.*

The disorientation distribution was similar to the analysis of the axial direction presented above and CSL fractions were very similar as well with largest fractions Σ3 and Σ9 twin boundaries. The fraction Σ3 was 48.5 % and Σ9 5.0 % which was a little less compared to the axial direction analysis. The fraction CSL were lower at the bottom side and centre (48 %) compared to the top side (50 %), this could explain why there was a difference between the axial section and the tangential. The axial section was taken from the mid-section of the lid.

It is possible to get the fractions of any crystallographic plane from EBSD data as shown earlier, and in this section it is interesting to analyse the top surface since this surface is the outer surface of the canister. The fractions were calculated with a 15° spread from the ideal orientation. The result of the analysis is presented in Figure 4-9. For the whole section close packed <111> planes were the most frequent with a fraction of 17.4 %, then <100> planes were second most frequent (14.7 %) and <110> planes the least frequent ones (14.2 %). The difference in occurrence between close packed planes was larger in this case compared to the mid-section as described above. The analysis showed that the top surface (left side) was more different with again the <111> plans most frequent with a fraction of 20.4 %, then <100> planes were second most frequent (16.0 %) and <110> planes the least frequent ones (11.2 %). At the canister inside surface (right) instead <110> plans most frequent with a fraction of 16.8 %, the <111> planes were second most frequent (15.2 %) and <100> planes the least frequent ones (13.4 %).

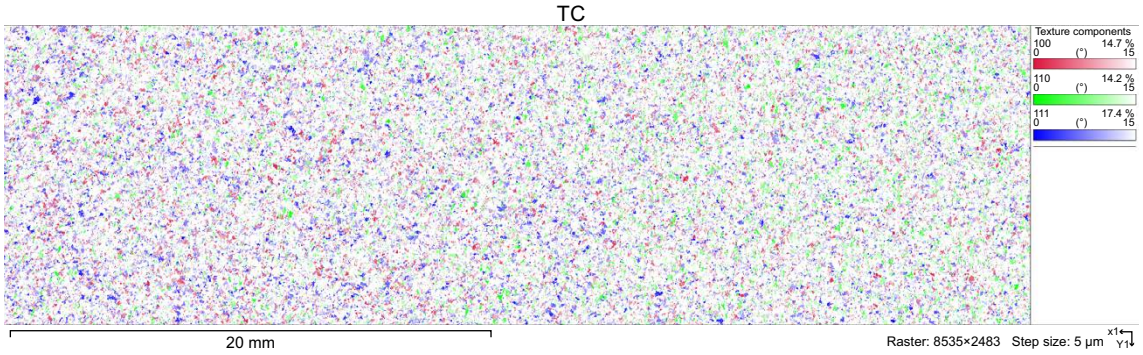

Figure 4-9. *Grain size analysis from the whole data set with 87 101 grains.*

4.3 Canister wall material

The canisters walls were analysed by ultrasonic sound before this study by SKB and areas with coarse and fine microstructures were identified. Three specimens were made from the tube T77 and 5 from the tube T101, one of the specimens from T77 and two from the T101 were taken from areas that were identified as having fine microstructures, the other specimens were taken from areas identified as coarse. Specimens were made for analysis in the three main directions in the wall, axial, tangential and radial. The axial and tangential specimens cover the entire section from the inside surface to the outside surface of the 50 mm thick wall, the radial instead origins from a defined depth in the wall. The large data set made it possible to analyse variations over the section and texture and grain sizes were analysed in this way.

4.3.1 T77 Axial direction, fine microstructure (specimen #1a, Table 4-2)

The axial section had the analysed surface-normal direction parallel to the axial direction in the canister. The long side (X) run parallel to the radial direction, from the inner surface to the outer surface. In Figure 4-10a–c the left side was at the outer surface and the right side the inner surface of the wall. Figure 4-10a–c shows the grains in the large area stitched EBSD map coloured with three different reference directions, axial (a) radial (b) and tangential (c). The difference that can be seen in colours indicates the presence of crystallographic texture in the material. The origin of texture is the thermo-mechanical processing which in this case was an extrusion process. In the axial direction (Z) red and blue colours were more frequent, red represents <100> planes and blue <111> planes. In the radial direction (X) green was more frequent which represents the <110> planes. In the tangential direction (Y) the colours were more mixed. Figure 4-11 shows the pole figures plotted with the acquisition axes as X, Y and Z, where Z is the axial direction, X is the radial and Y is the tangential direction. X is also the normal direction in the extruded tube. The maximum texture strength was 5.5 times random in this analysis and the strongest peak was the <100> planes in axial direction. The texture was stronger in the wall material compared to the lid. The left side (outer surface) of the canister show more frequent large grains.

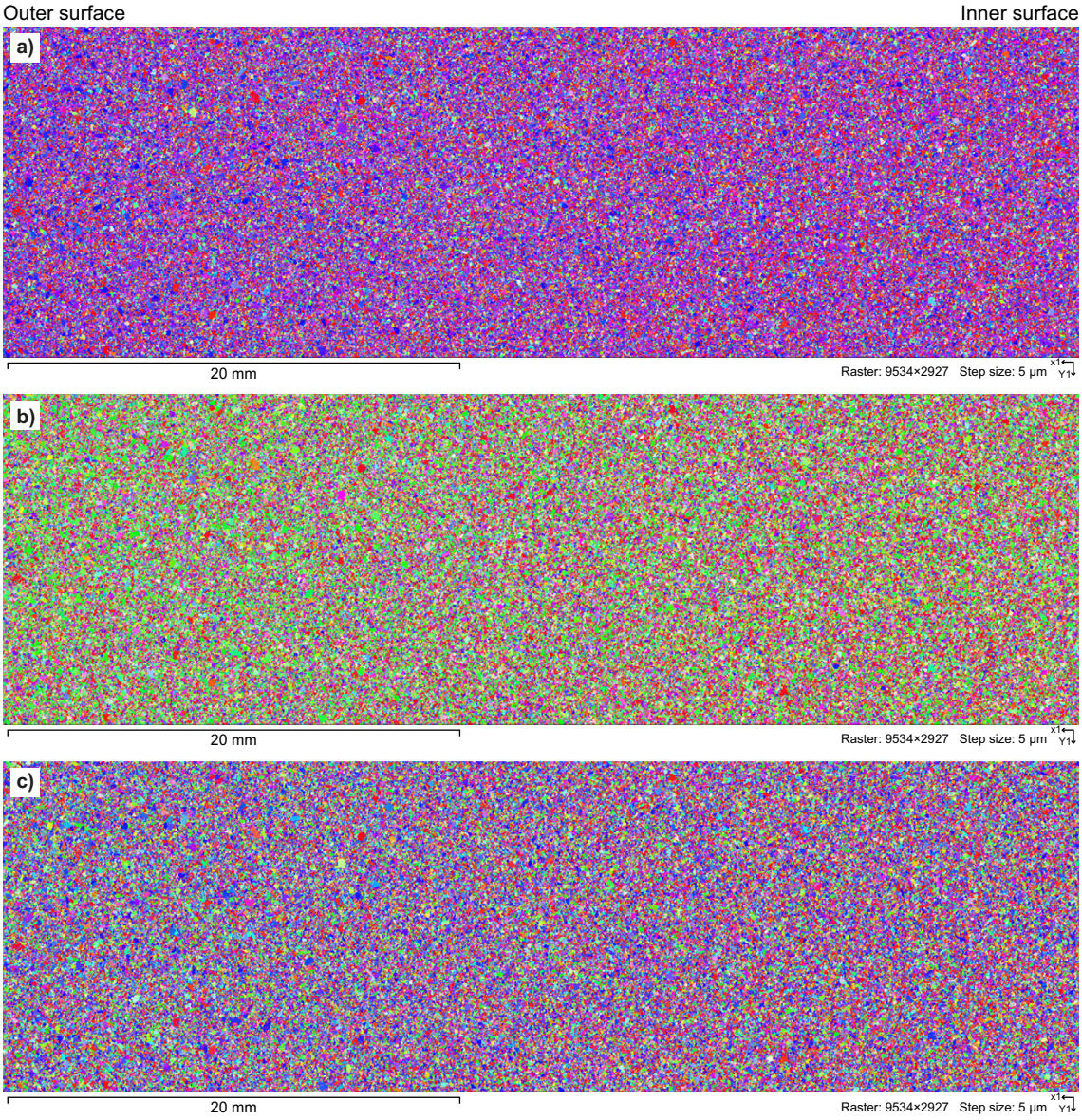

Figure 4-10. *EBSD analysis in axial direction in canister wall T77. Analysis was made from the inner surface (right) to the outer surface (left). The colours show crystal orientations in three directions, Z (axial), X (radial) and Y (tangential).*

The IPF colours in all directions did not show significant variation over the section which indicates small variations in texture. The pole figure for the complete data set is shown in Figure 4-11a, the <100> peak parallel to the axial direction was the strongest texture peak and was similar over the complete section 5.5 times random. The texture was not completely symmetric for the complete data set, which probably relates to friction in the tools during extrusion. Close to the outer surface, pole figures in Figure 4-11b the texture was however symmetric. <111> grains were more frequent at the left side (close to outer surface).

The grain size analysis showed that the data set contains 157 249 grains, a graph is shown in Figure 4-12. The threshold for grain boundaries was set to 10° disorientation and the Σ3 and Σ9 twins were excluded in the analysis. The arithmetic mean diameter in the complete data set was 66 µm and the area weighted mean diameter was 125 µm, the largest grain diameter was 465 µm. Analysis of the grain size change from left to right showed that the distribution of size changed with more large grains on the left side but the arithmetic mean diameter did not change a lot. The arithmetic mean actually increased from left to right, from 61.5 mm to 69.6 µm, when at the same time the area weighted mean showed close to average mean diameters at both inner and outer surfaces (124 µm) and then a peak at 25 % depth from left to about the centre (129 µm) and a minimum at 75 % depth (118 µm). The largest grains were more frequent at the left side (close to canister outer surface) with several grains larger than 600 µm. At the right side the grains were smaller, the largest grains had diameters around 380 µm.

Figure 4-13 shows the disorientation distribution in the analysed data set. The threshold was set to 2°, a threshold was necessary to cut away measuring noise and 2 degrees threshold was used for all data sets in this work. The peak at 60° show the Σ3 twin boundaries, and the peak at 39° are related to the Σ9 boundaries. The peak at low boundaries that was seen in the data from top-sealing lid material was not present in this material (and not in any analysis from the tube walls). The absence of low angle (dislocation) boundaries tells us that the material was completely recrystallised.

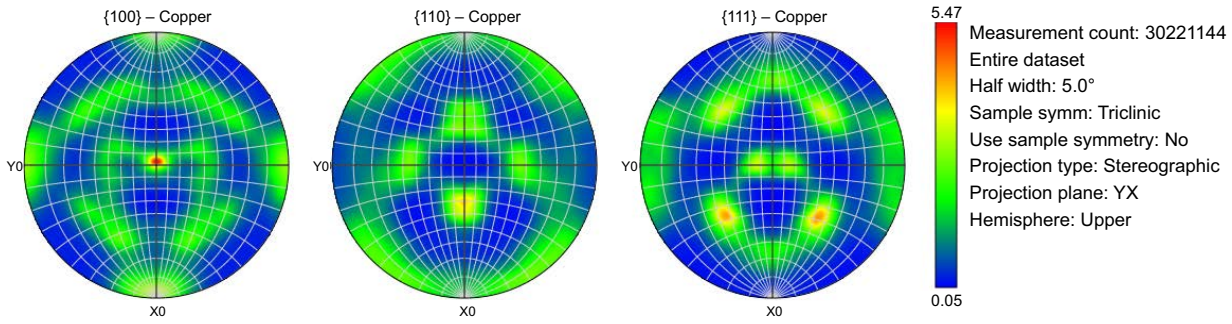

Figure 4-11a. *Pole figure from the complete data set.*

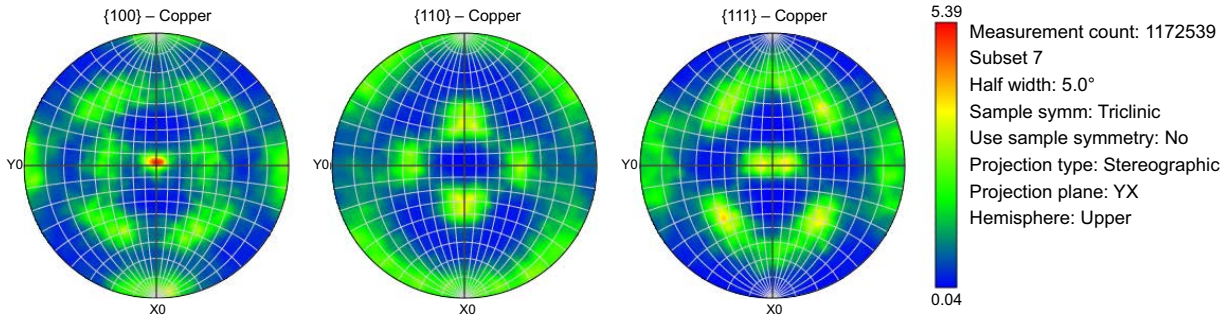

Figure 4-11b. *Pole figure from the outer surface region.*

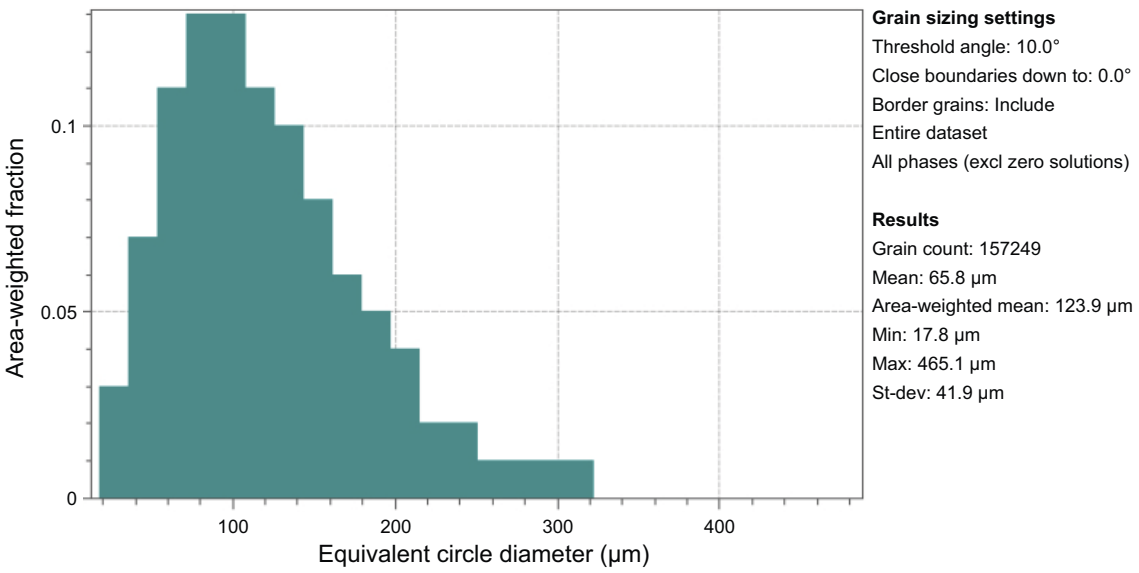

Figure 4-12. *Grain size distribution in canister T77 wall measured in the axial direction. 157249 grains were included in the analysis.*

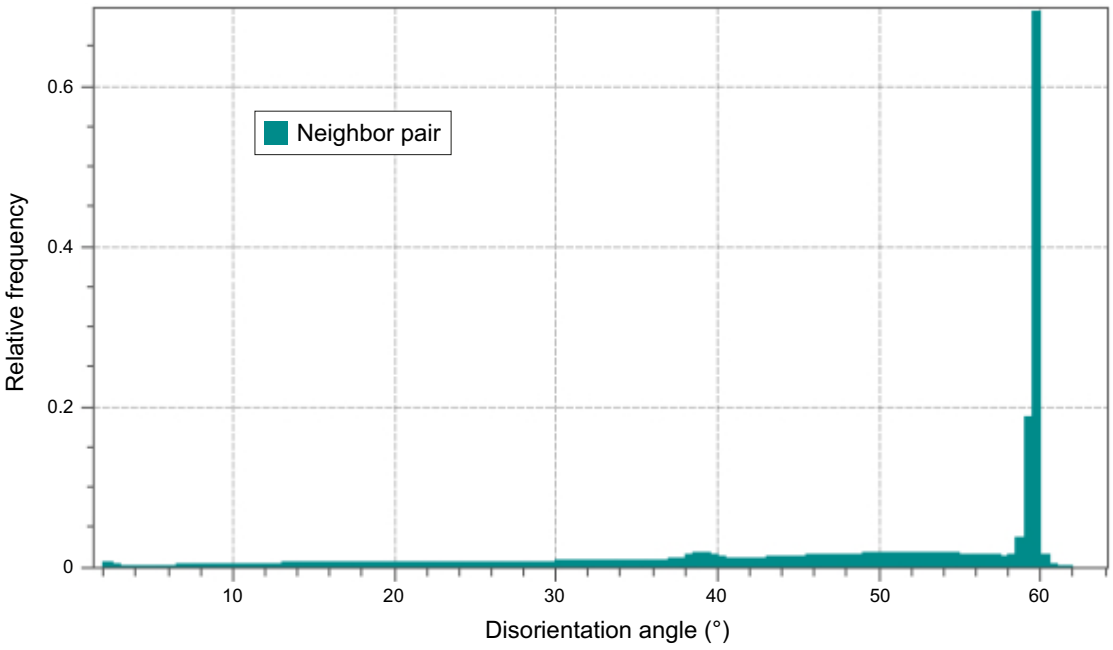

Figure 4-13. *Disorientation distribution in canister T77 wall measured in the axial direction.*

4.3.2 T77 Tangential direction, coarse microstructure (specimen #4, Table 4-2)

Figure 4-14 shows the grains in the large area stitched EBSD map measured on section with the normal direction in the tangential direction. The long side (X) run parallel to the radial direction, from the inner surface to the outer surface. In Figure 4-14 the left side was at the outer surface and the right side the inner surface of the wall. The colours show crystal orientations with reference to the axial direction. Figure 4-15 shows the pole figures plotted with the acquisition axes as X, Z and Y, where X is the radial direction, Z is the tangential direction and Y is the axial direction. X is also the thickness direction in the extruded tube. The texture strength was 5.5 in this analysis, which was similar to the texture strength in the analysis of the axial section. The strongest peak was the <100> planes in axial direction. The texture was stronger in the wall material compared to the lid. Texture strength did not change significantly from left to right, but large blue coloured grains were more frequent at the left side. In general, large grains were more frequent at the left side, which was in agreement with the analysis on the section in the axial direction.

The grain size analysis showed that the data set contained 150 508 grains, Figure 4-16. The threshold for grain boundaries was set to 10° disorientation and the Σ3 and Σ9 twins were excluded in the analysis. The arithmetic mean diameter was 66 µm and the area weighted mean diameter was 124 µm, the largest grain had a diameter of 617 µm. Analysis of the grain size from left to right showed that the distribution of size changed with more large grains on the left side. The arithmetic mean diameter showed a different behaviour, it actually increased from left to right, from 61.5 mm to 69.6 µm. At the same time the area weighted mean varied in a more complex way, with about average mean diameters close to both surfaces (124 µm) and then a peak at 25 % depth from left to about the centre (129 µm) and a minimum at 75 % depth (118 µm). The largest grains were more frequent at the left side with grains larger than 600 µm. At the right side the grains were smaller, the largest grains had diameters around 380 µm. This variation in grain size was similar in the previous analyses on the section in axial direction.

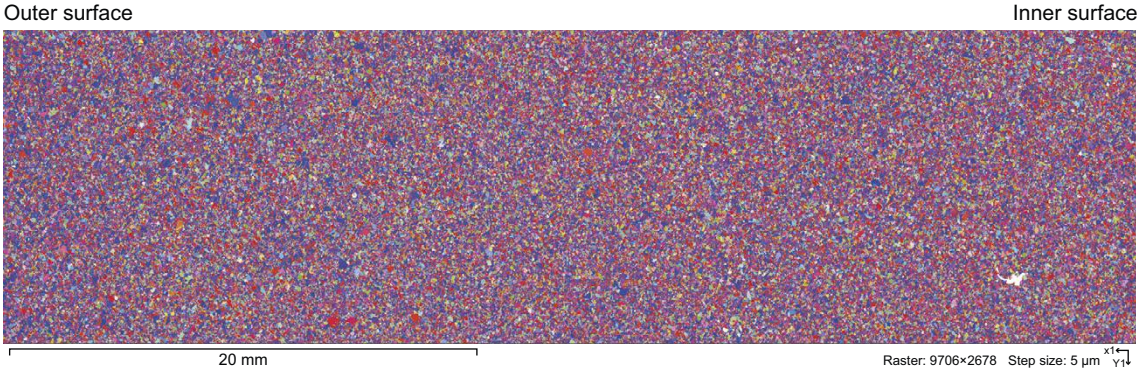

Figure 4-14. *EBSD analysis in tangential direction in canister wall T77. Analysis was made from inner surface (right) to outer surface (left). The colours show the crystal orientation in the axial direction.*

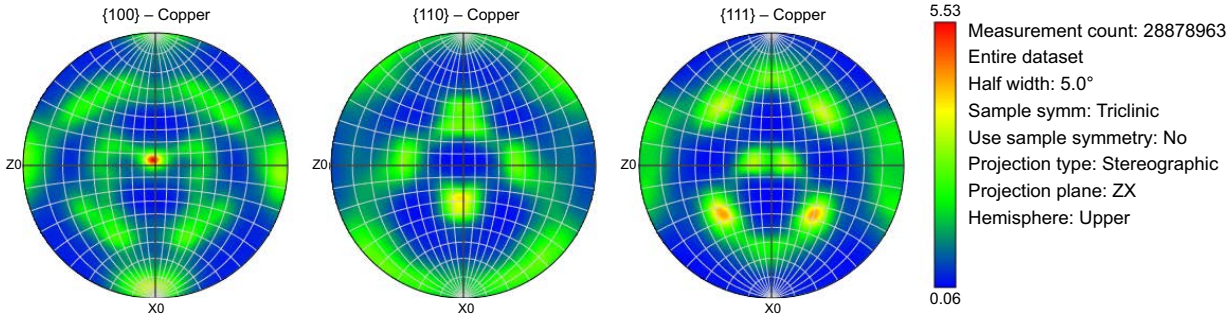

Figure 4-15. *Pole figure from the complete data set.*

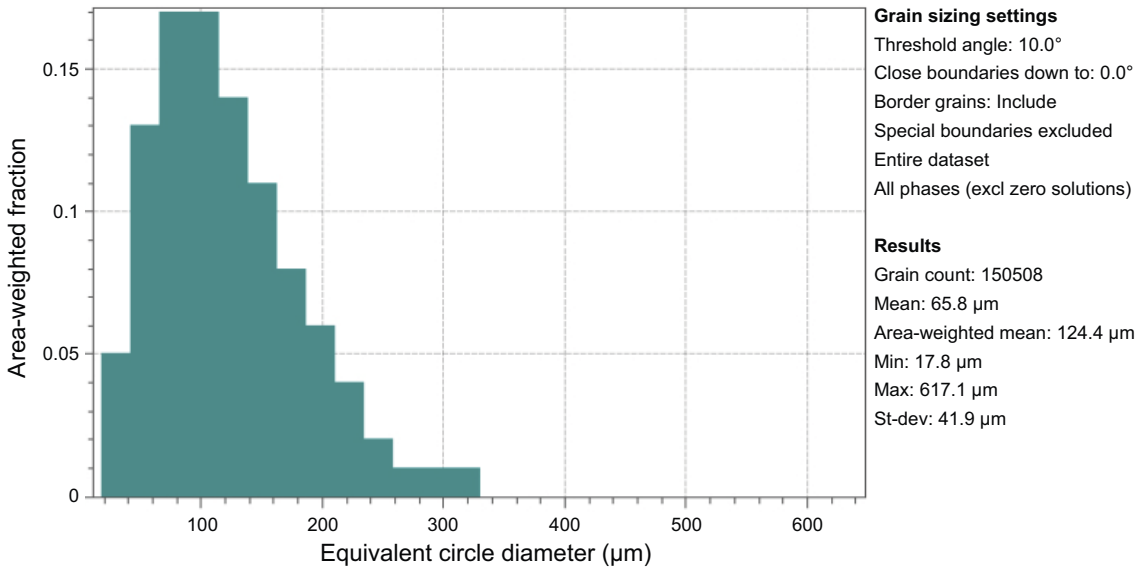

Figure 4-16. *Grain size distribution in canister T77 wall measured in the tangential direction. 150508 grains were included in the analysis.*

4.3.3 T77 radial direction, half depth, coarse microstructure (specimen #6, Table 4-2)

The radial section had the long side (X) parallel to the axial direction and short side parallel to the tangential direction. The acquisition area normal direction (Z) was parallel to the radial direction. The analysed surface origin was from half thickness in the wall. Figure 4-17 shows the grains in the large area stitched EBSD map coloured with reference to the axial direction. Following the pattern from the previous analyses the cube orientation, <100> plane normal parallel to the axial direction were dominating the picture (red colour). Figure 4-18 shows the pole figures plotted with the acquisition axes as Y, Z and X. X was aligned to the axial direction. Z was equal to the radial direction and Y was aligned to the tangential direction. Z is also the thickness direction in the extruded tube. The texture strength was 4.5 in this analysis and the strongest peak was the <100> planes in axial direction. The texture was stronger in the wall material compared to the lid. Texture strength did not change significantly from left to right. This analysis agrees very well to the previous ones made on sections in axial- and tangential directions, the grain size distribution with more frequent large grains look similar to the mid-section in the previous analyses which covered the surface from the inner to the outer surfaces in the canister wall.

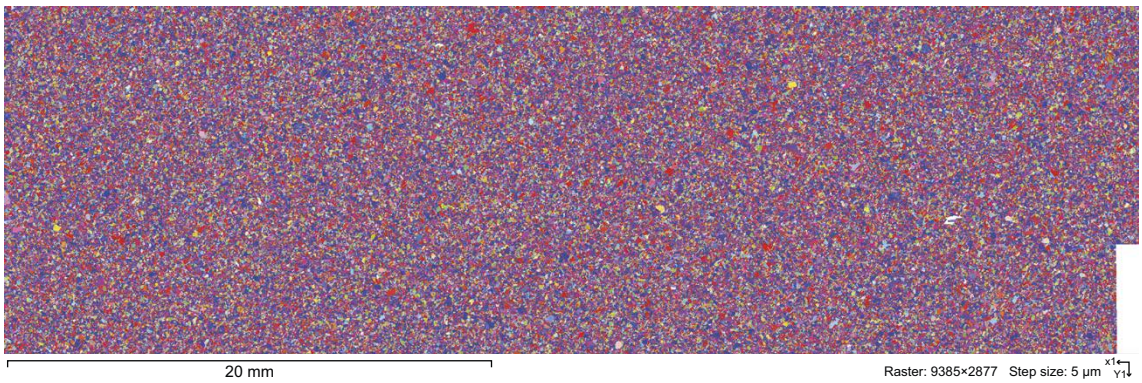

Figure 4-17. *EBSD analysis in radial direction at half thickness in canister wall T77. The colours show the crystal orientation in the axial direction (X). The strongest peak was <100> planes in the axial direction.*

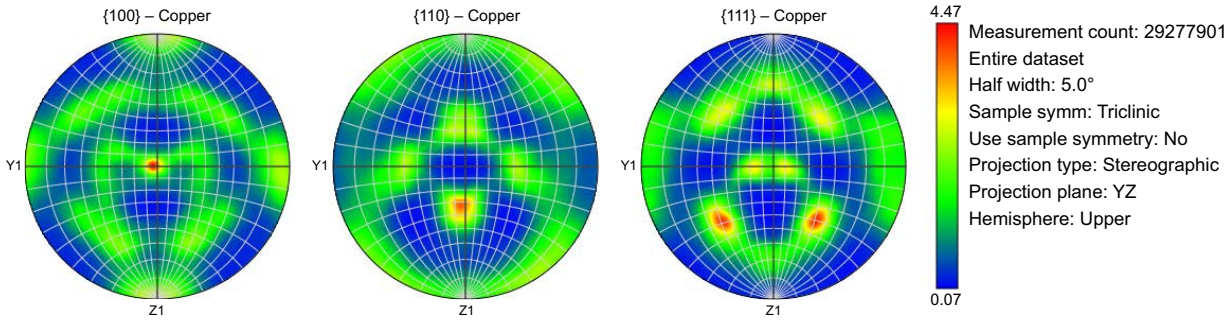

Figure 4-18. *Pole figure from the complete data set.*

The data set contained 161 772 grains. The threshold for grain boundaries was set to 10° disorientation and the Σ3 and Σ9 twins were excluded in the analysis. Figure 4-19 shows the grain size distribution in the complete section. The arithmetic mean diameter was 64 µm and the area weighted mean diameter was 119 µm, the largest grain had a diameter of 533 µm. Analysis of the grain size from left to right showed that the distribution of size was quite the same over the section, the arithmetic mean diameter did not change a lot. The area weighted mean was a bit larger at the right side 121 µm compared to 118 µm at the left side. Overall, the grain size distribution was similar over the section. The section was from the mid-thickness of the wall and it was expected to see the same grain size and texture over the complete section. Figure 4-20 shows the disorientation distribution, same result as in the previous analyses with no LAGB and peaks for Σ3 and Σ9 boundaries.

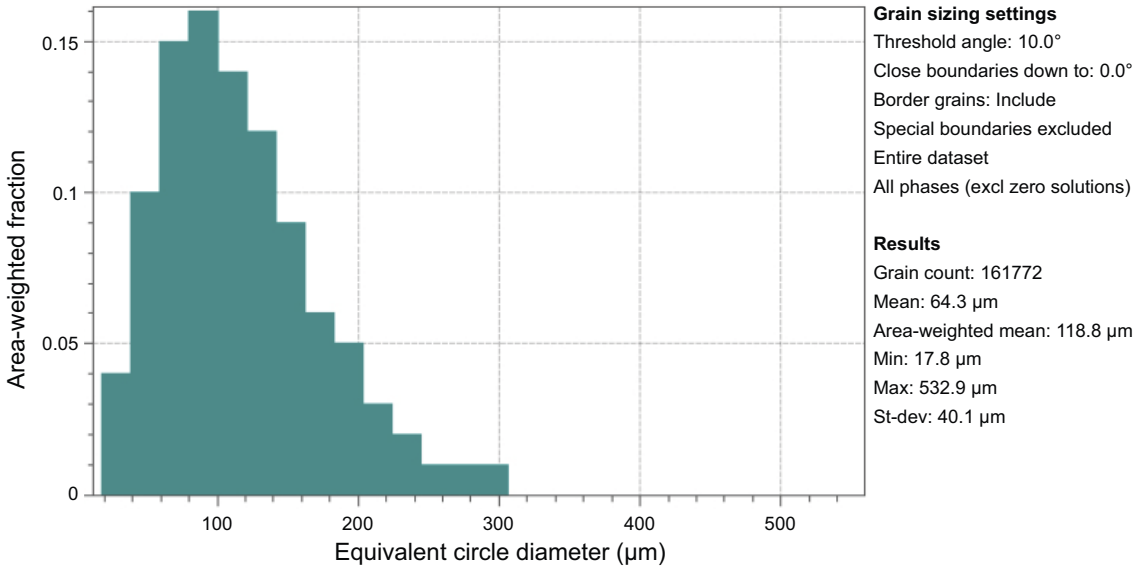

Figure 4-19. *Grain size distribution in canister T77 wall measured in the radial direction. 161 772 grains were included in the analysis.*

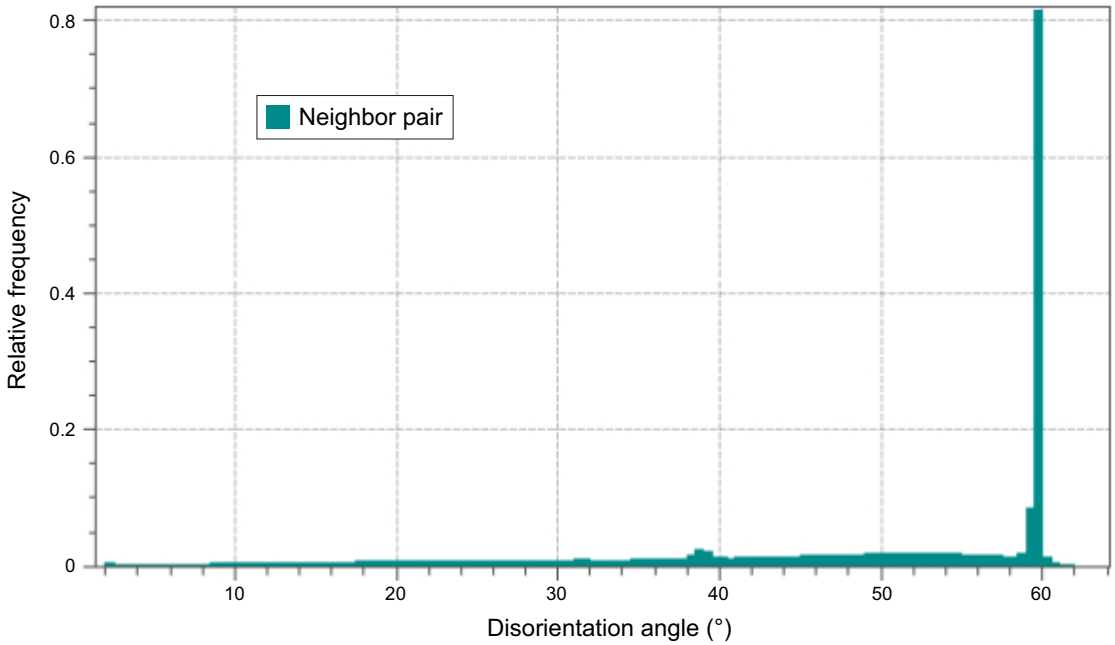

Figure 4-20. *Disorientation distribution in canister T77 wall measured in the radial direction.*

4.3.4 T101 Axial direction, coarse microstructure (specimen #2, Table 4-2)

The axial section in the canister tube wall had the analysed surface normal direction parallel to the axial direction in the canister. The long side (X) run parallel to the radial direction, from the inner surface to the outer surface. In Figure 4-21a–c the right side was at the outer surface and the left side the inner surface of the wall (inverted to the previous analyses, and to Figure 2-1). The figure shows the grains in the large area stitched EBSD map coloured with reference to the main three directions, axial (a) radial (b) and tangential (c). The difference that can be seen in colours indicates the presence of crystallographic texture in the material. In the axial direction (Z) red and blue colours were more frequent, red represents <100> planes and blue <111> planes. In the radial direction (X) green was more frequent which represents the <110> planes. In the tangential direction (Y) the colours were more mixed. X also represents the thickness direction in the tube wall. The right side (outer surface) of the canister showed more frequent large grains.

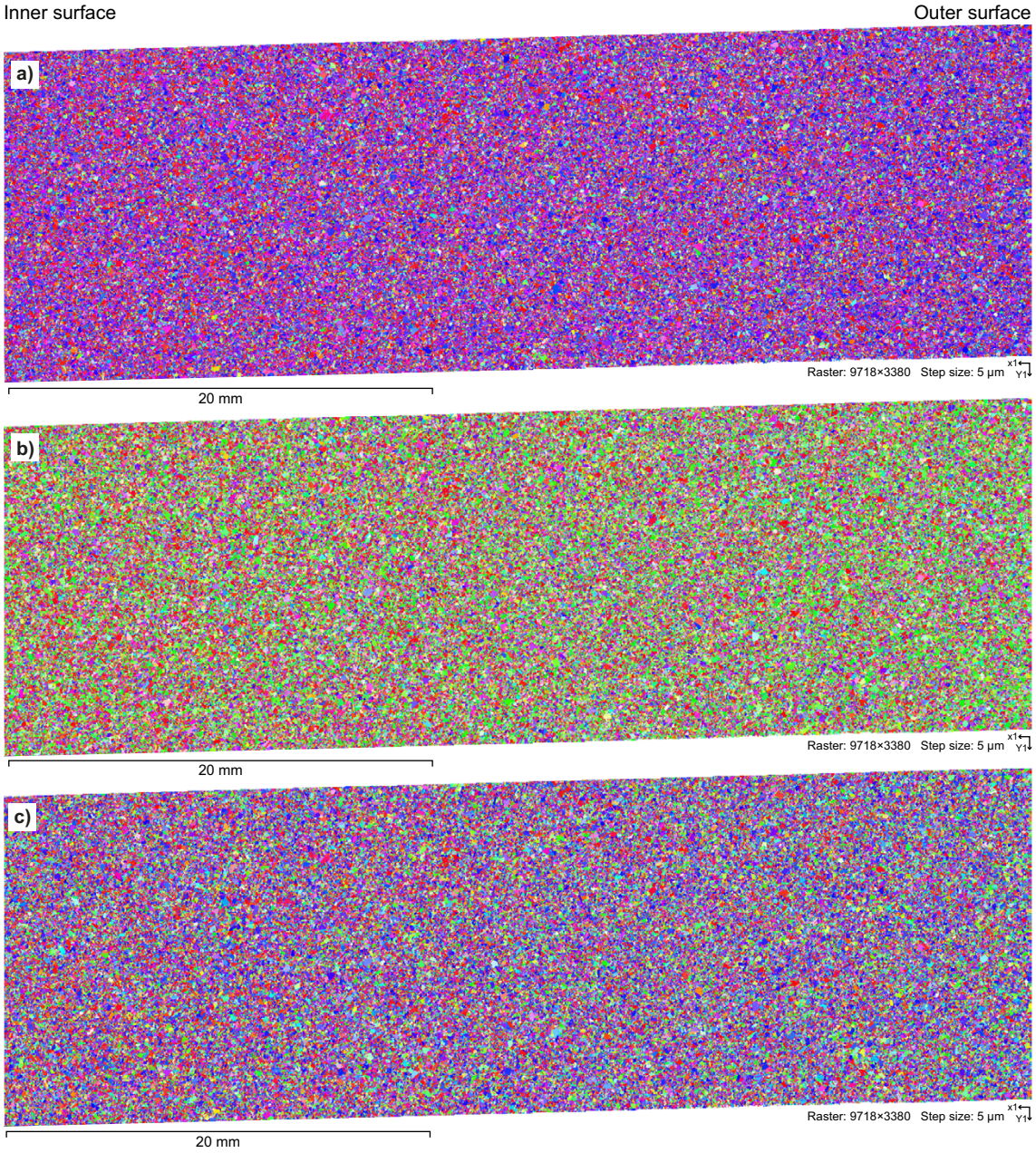

Figure 4-21. *EBSD analysis in axial direction in canister wall T101. The colours show the crystal orientation in the three main directions, axial (a), radial (b) and tangential (c).*

Pole figures are given in Figure 4-22a–c. The texture strength was 5.3 in this analysis for the complete data set, and the strongest peak was the <100> planes in axial direction. The texture was stronger in the wall material compared to the lid. The IPF colours did not show a strong variation over the section which indicates small variations in texture. The texture was not completely symmetric, which can be seen in the <100> Pole figure for the complete data set. The texture strength was higher at the inner surface (Figure 4-22b), Close to the outer surface, pole figures in Figure 4-22c, the texture was however symmetric. <111> grains were more frequent at the outer surface which can be seen also in the <111> pole figure where the peak in the middle is stronger compared to the complete data set.

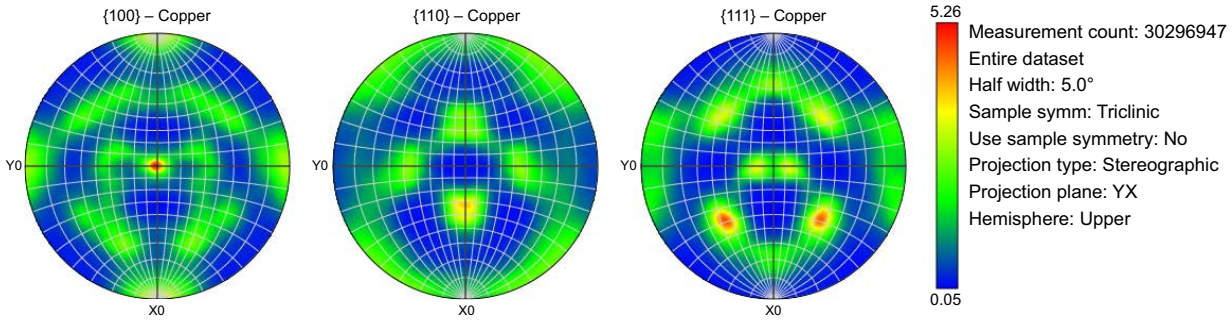

Figure 4-22a. *Pole figure from the complete data set.*

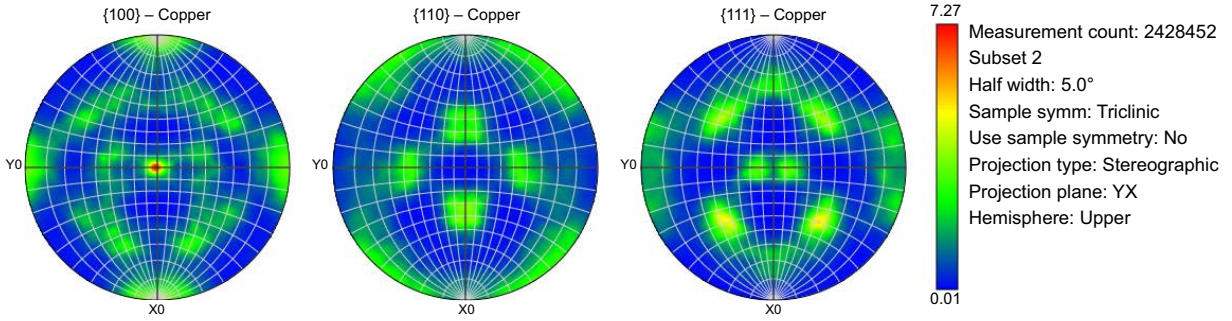

Figure 4-22b. *Pole figure from the inner surface.*

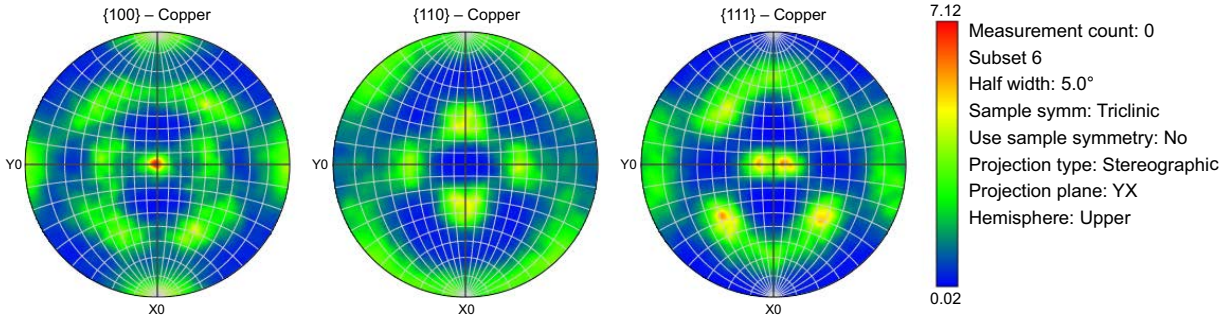

Figure 4-22c. *Pole figure from the outer surface.*

The data set contained 125 968 grains. The threshold for grain boundaries was set to 10° disorientation and the Σ3 and Σ9 twins were excluded in the analysis. Figure 4-23 shows the grain size distribution in the complete section. The arithmetic mean diameter was 73 µm and the area weighted mean diameter was 142 µm, the largest grain had a diameter of 532 µm. Analysis of the grain size from left to right showed that the distribution of size was quite the same over the section, the arithmetic mean diameter did not change a lot, 72 µm ± 3 µm. The area weighted mean varied similarly to the earlier analysis with a maximum at 25 % depth (inner, 145 µm) and a minimum at 25 % (outer, 138 µm). Overall, the grain size distribution was similar over the section. Figure 4-24 shows the disorientation distribution, same result as in the previous analyses with no LAGB and peaks for Σ3 and Σ9 boundaries.

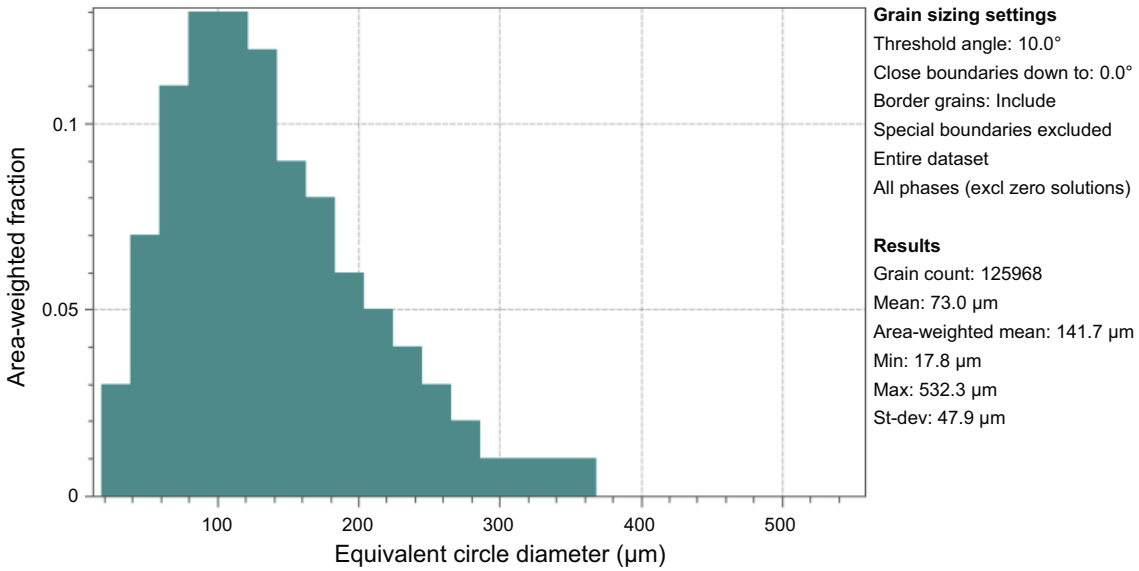

Figure 4-23. *Grain size distribution in canister T101 wall measured in the radial direction. 125 968 grains were included in the analysis.*

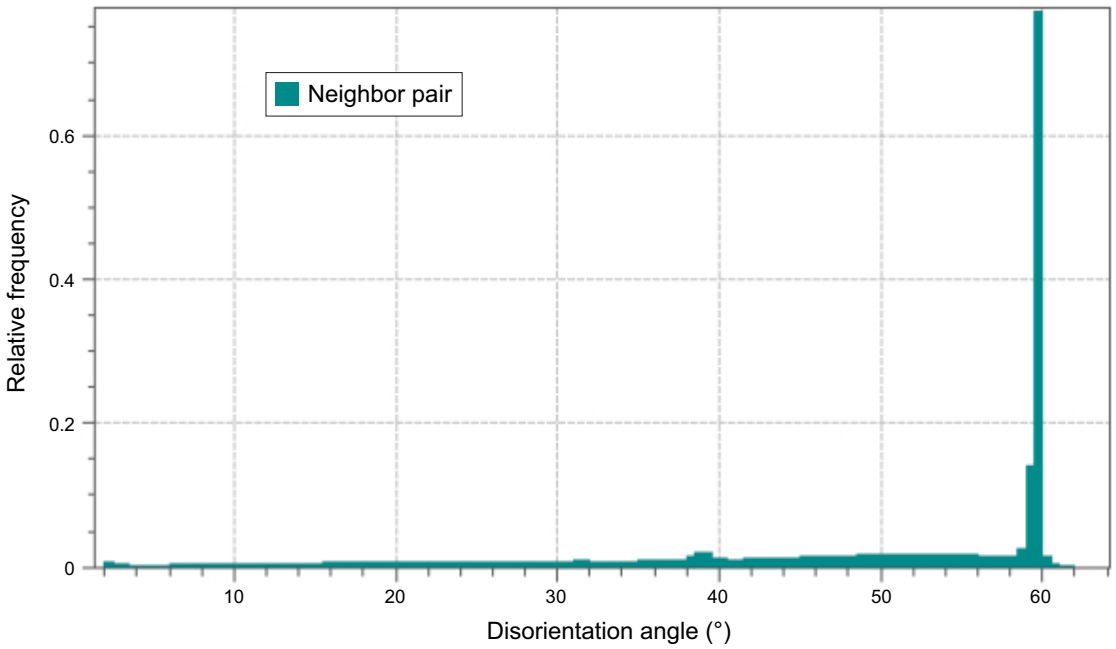

Figure 4-24. *Disorientation distribution in canister T101 wall measured in the axial direction.*

4.3.5 T101 Axial direction, fine microstructure (specimen #1b, Table 4-2)

The axial section in the canister tube wall had the analysed surface normal direction parallel to the axial direction in the canister. The long side (X) run parallel to the radial direction, from the inner surface to the outer surface. In Figure 4-25 the left side was at the outer surface and the right side the inner surface of the wall. The figure shows the grains in the large area stitched EBSD map coloured with reference to the axial direction. Red and blue colours were more frequent, red represents <100> planes and blue <111> planes. X also represents the thickness direction in the tube wall. In this section it was difficult to judge just from the EBSD map if any of the two sides contained more large grains. The outer surface of the canister showed more frequent large grains for the previous analyses. The same trend with more blue <111> grains was the same, the outer surface (left) side in the map below show more blue grains. Figure 4-26a shows the pole figures from the complete map. The same results as for previous maps was seen for this analysis. The outer surface texture was a bit weaker and symmetric as seen in Figure 4-26b. The inner surface texture was stronger (6.6 times random) and showed the same asymmetry as the complete data set pole figures.

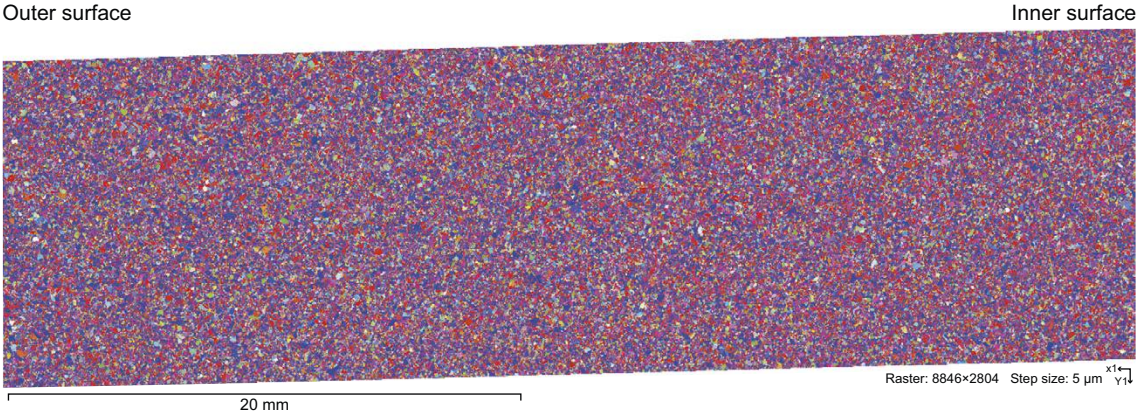

Figure 4-25. *EBSD analysis in axial direction in canister wall T101 having been pre-determined ultrasonically to have fine microstructure. The colours show the crystal orientation in the axial direction (Z). The image is a rectangular sub-set from the original data set.*

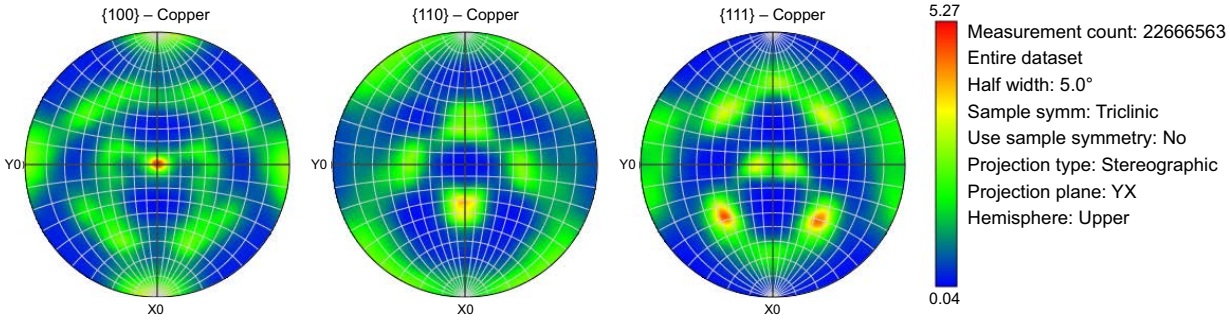

Figure 4-26a. *Pole figure from the complete data set.*

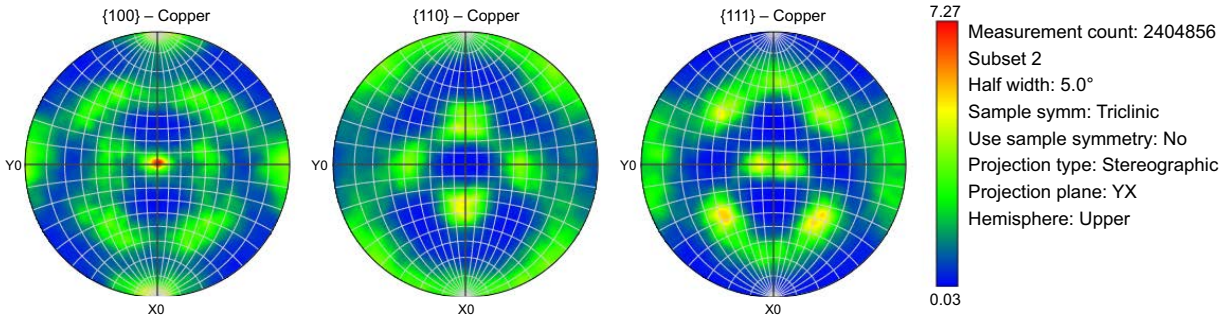

Figure 4-26b. *Pole figure from the outer surface region.*

The data set contained 106 830 grains. The threshold for grain boundaries was set to 10° disorientation and the Σ3 and Σ9 twins were excluded in the analysis. Figure 4-27 shows the grain size distribution in the complete section. The arithmetic mean diameter was 69 µm and the area weighted mean diameter was 131 µm, the largest grain had a diameter of 459 µm. The microstructure was finer than the previous which is in agreement with the ultrasonic measurements. Analysis of the grain size from left to right showed that the distribution of size was quite the same over the section, the arithmetic mean diameter did not change a lot, 68 µm ± 3 µm. The area weighted mean varied similarly to the earlier analysis with a maximum at 25 % depth (135 µm). Overall, the grain size distribution was similar over the section.

Figure 4-28 shows the disorientation distribution, same result as in the previous analyses with no LAGB and peaks for Σ3 and Σ9 boundaries.

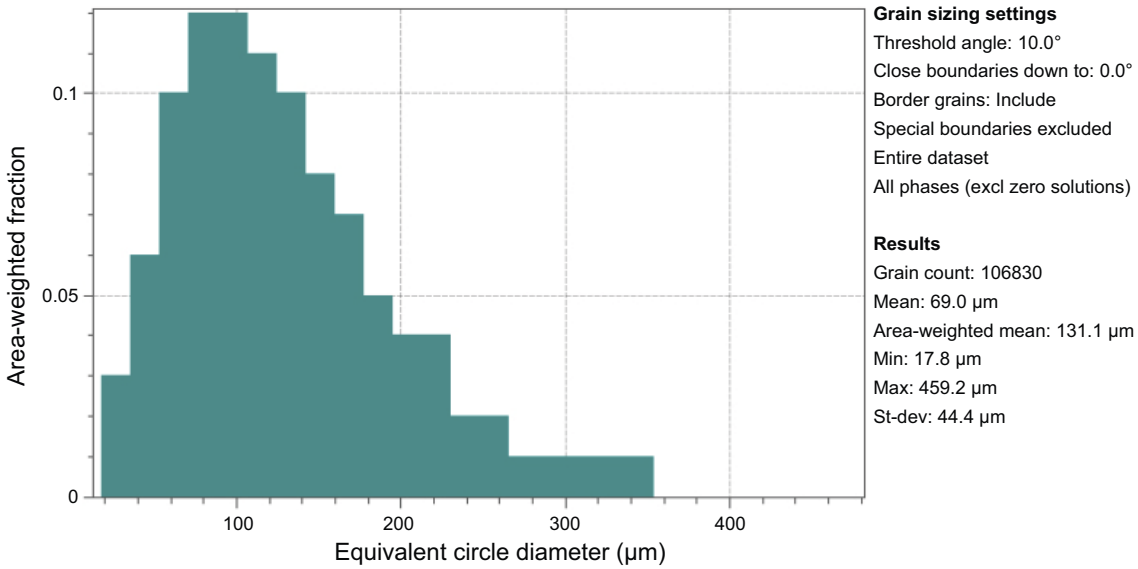

Figure 4-27. *Grain size distribution in canister T101 wall measured in the axial direction. 106 830 grains were included in the analysis.*

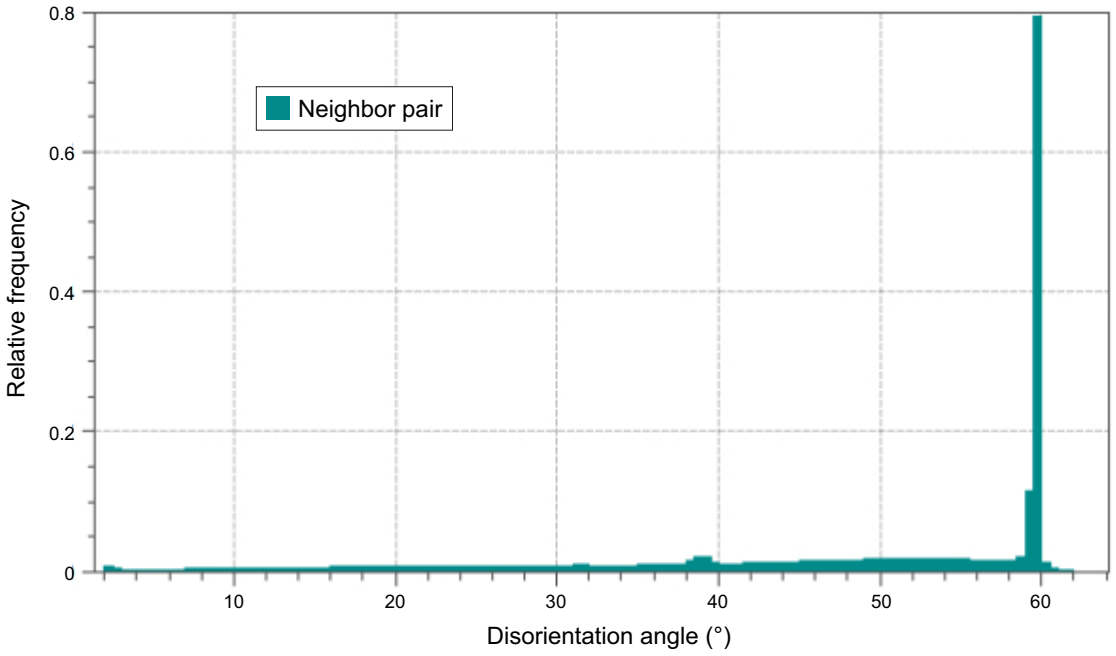

Figure 4-28. *Disorientation distribution in canister T101 wall measured in the axial direction.*

4.3.6 T101 Tangential direction, fine microstructure (specimen #3, Table 4-2)

Figure 4-29 shows the grains in the large area stitched EBSD map measured on a section with the normal direction in the tangential direction. The long side (X) run parallel to the radial direction, from the inner surface to the outer surface. In Figure 4-29 below the right side was at the outer surface and the left side the inner surface of the wall (inverted compared to Figure 2-1). The colours show crystal orientations with reference to the axial direction. Figure 4-30 shows the pole figures plotted with the acquisition axes as X, Z and Y, where X is the radial direction, Z is the tangential direction and Y is the axial direction. X is also the thickness direction in the extruded tube. The texture strength was 5.6 in this analysis, which was similar to the texture strength in the analysis of the axial section. The strongest peak was the <100> planes in axial direction. The texture was stronger in the wall material compared to the lid. Texture strength did not change very much from left to right, but large blue coloured grains were more frequent at the right side. In general, large grains were more frequent at the outer surface (right) side, which agreed with the analysis on the section in the axial direction.

The grain size distribution for the canister wall T101 measured on the tangential section is shown in Figure 4-31. 126421 grains were included in the analysis. The threshold for grain boundaries was set to 10° disorientation and the Σ3 and Σ9 twins were excluded in the analysis. The arithmetic mean diameter was 69 µm and the area weighted mean diameter was 131 µm, the largest grain had a diameter of 499 µm. Analysis of the grain size from left to right showed that the distribution of size was quite the same over the section, the arithmetic mean diameter did not change a lot, 69 µm ± 3 µm. The area weighted mean varied similarly to the earlier analysis with a maximum at 25 % depth (134 µm). Overall, the grain size distribution was similar over the section. Large grains were more frequent at the outer surface, but at the same time the arithmetic mean diameter was smaller, 66 µm, compared to the inner side with 69 µm. Figure 4-32 shows the disorientation distribution, same result as in the previous analyses with no LAGB and peaks for Σ3 and Σ9 boundaries.

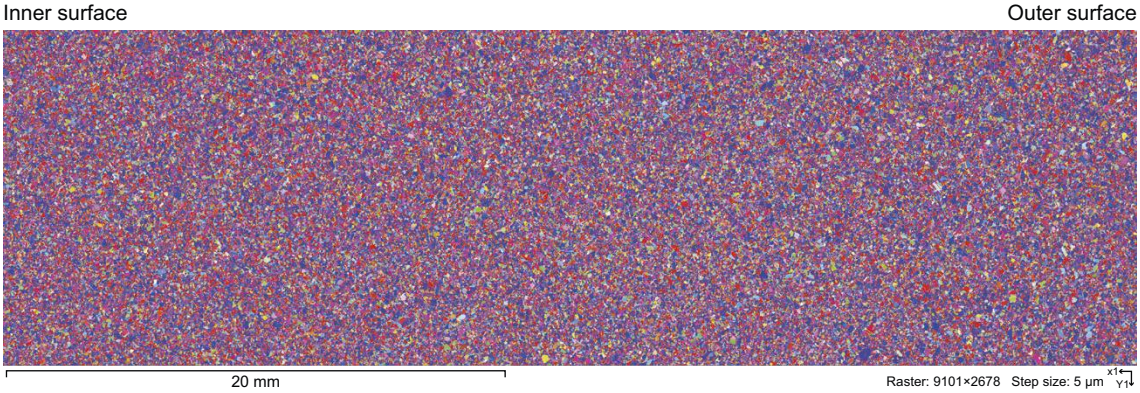

Figure 4-29. *EBSD analysis in tangential direction in canister wall T101. Analysis was made from inner surface (left) to outer surface (right). The colours show the crystal orientation in the axial direction (Y). The image is a rectangular sub-set from the original dataset.*

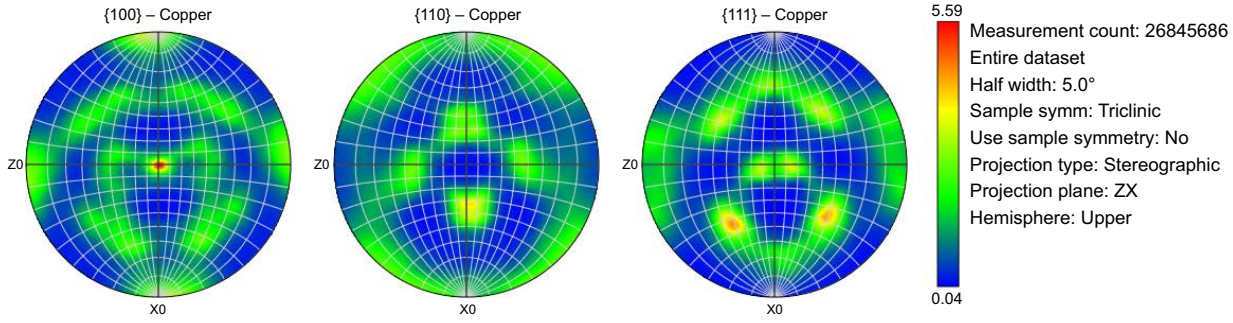

Figure 4-30. *Pole figure from the complete data set.*

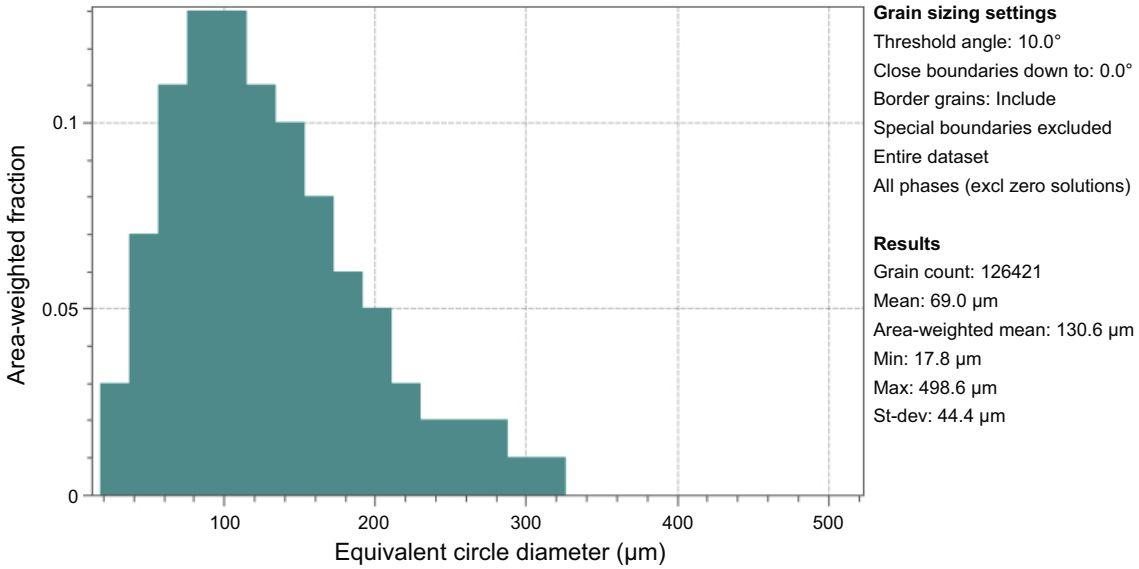

Figure 4-31. *Grain size distribution in canister T101 wall measured in the tangential direction. 126 421 grains were included in the analysis.*

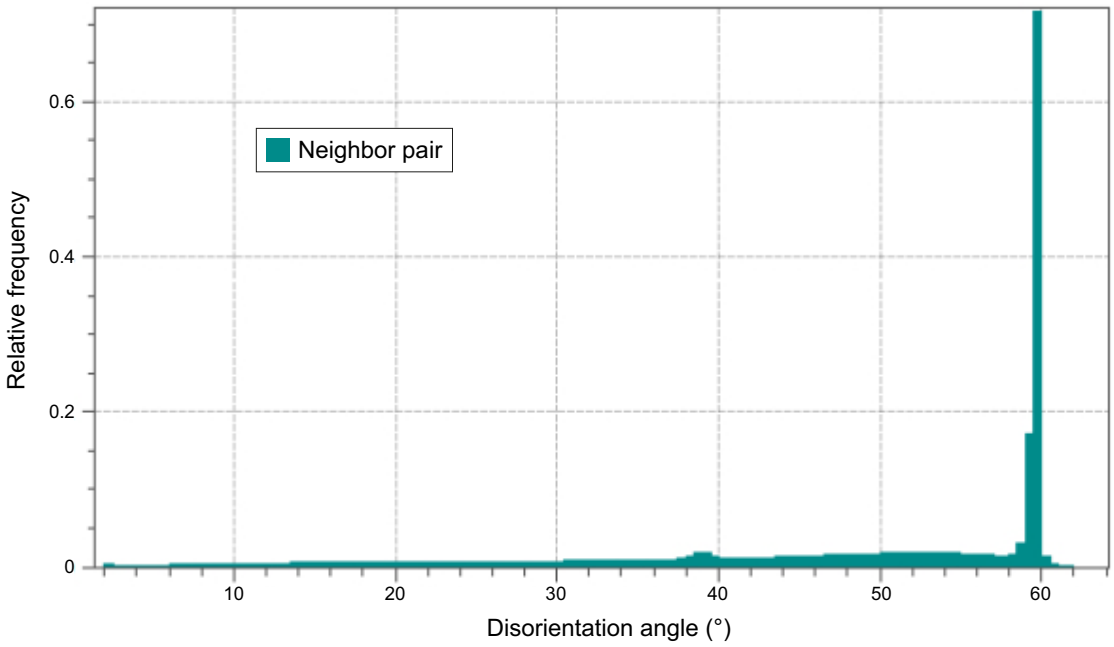

Figure 4-32. *Disorientation distribution in canister T101 wall measured in the tangential direction.*

4.3.7 T101 Radial direction, Outer surface, Fine microstructure (specimen #5, Table 4-2)

The radial section had the long side (X) parallel to the axial direction and short side parallel to the tangential direction. The acquisition area normal direction (Z) was parallel to the radial direction. The analysed surface origin was from the tube outer surface. Figure 4-33a,b shows the grains in the large area stitched EBSD map coloured with reference to the axial direction (a) and the radial direction (b). Following the pattern from the previous analyses the cube orientation, <100> plane normal parallel to the axial direction were dominating the picture (red colour), but <111> grains (blue) were also present. In the radial direction instead the <110> planes dominate the picture (green) together with the <100> planes (red). Figure 4-34 shows the pole figures plotted with the acquisition axes as Y, Z and X. X was aligned to the axial direction. Z was equal to the radial direction and Y was aligned to the tangential

direction. Z is also the thickness direction in the tube wall. Close packed crystal planes parallel to the outer surface are of interest in corrosion modelling and this is the planes with their normal parallel to the radial direction. An evaluation of fractions of such planes are shown in Figure 4-35.

The texture strength was 4.8 in this analysis and the strongest peak was the <100> planes in axial direction. The pole figures were in this case very symmetric, which agrees with previous results where the subsets at the outer surface always were more symmetric compared to the centre and at the inner surface. Texture strength did not change significantly from left to right which was expected since the analysed surface was from a certain depth within the wall (close to the canister outer surface). The grain size distribution with frequent large grains looks similar to the near surface part in the previous analyses which covered the surface from the inner to the outer surfaces in the canister wall. Green <110> grains were dominating the image of IPF colouring in the radial direction.

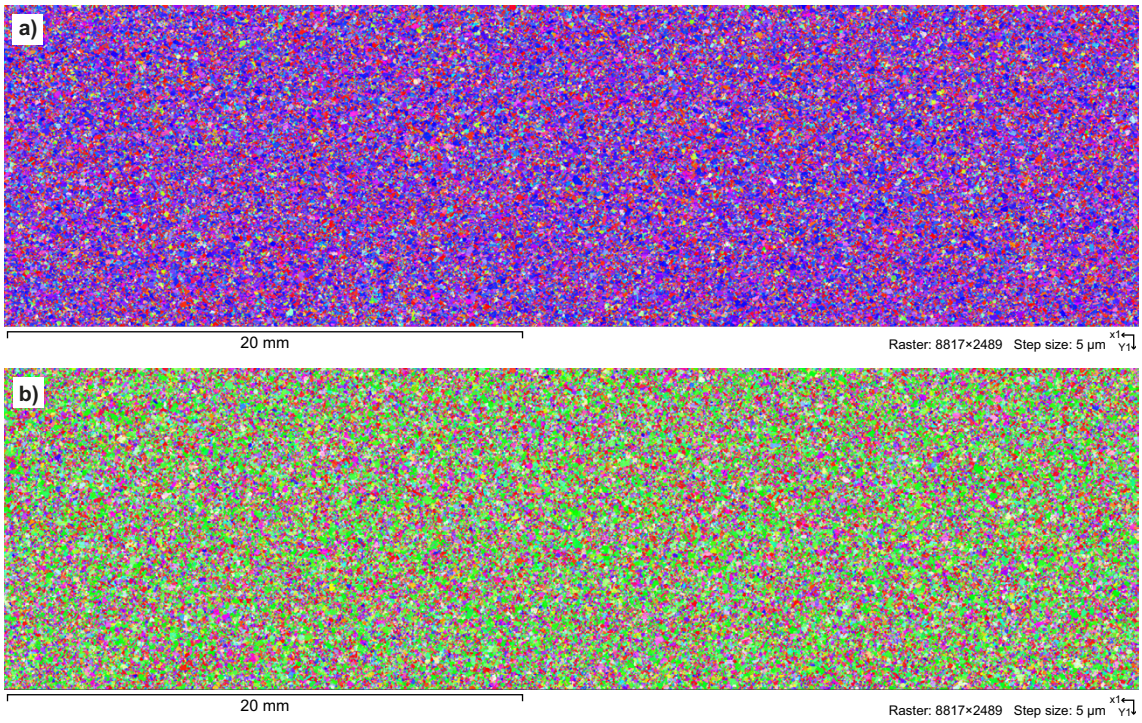

Figure 4-33. *EBSD analysis in radial direction in canister wall T101 close to the outer surface. The colours show the crystal orientation in the axial direction (a) and the radial direction (b). The image is a rectangular sub-set from the original dataset.*

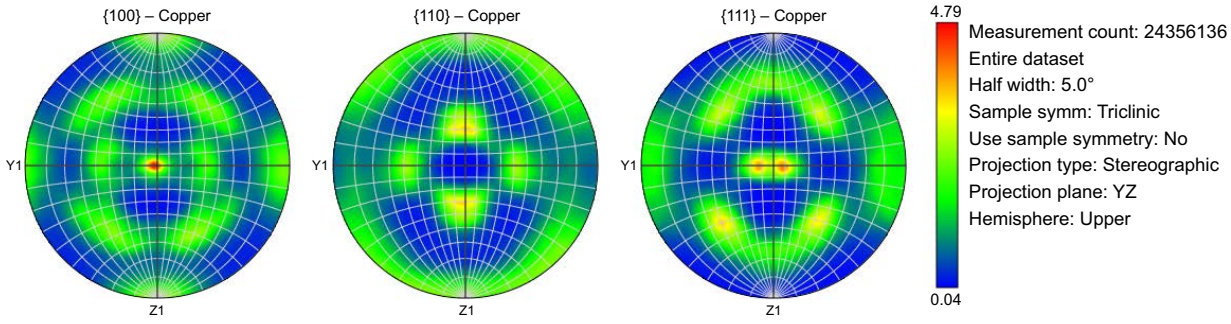

Figure 4-34. *Pole figure from the complete data set.*

The fractions of close packed planes parallel to the outer surface was evaluated with 15° spread. In Figure 4-35 the results are shown, and it was learned that the <110> had largest presence with 31.4 % in this case. <100> planes were almost 15 % and <111> grains only 5.6 %.

The grain size distribution for the canister wall T101 measured on the radial section is shown in Figure 4-36. 112 583 grains were included in the analysis. The threshold for grain boundaries was set to 10° disorientation and the Σ3 and Σ9 twins were excluded in the analysis. The arithmetic mean diameter was 68 µm and the area weighted mean diameter was 139 µm, the largest grain had a diameter of 493 µm. Analysis of the grain size from left to right showed that the distribution of size was quite the same over the section, the arithmetic mean diameter did not change a lot, 69 µm ± 3 µm. The area-weighted mean varied similarly to the earlier analysis with a maximum at 25 % depth (134 µm). Overall, the grain size distribution was similar over the section. Large grains were more frequent at the outer surface, but at the same time the arithmetic mean diameter was smaller, 66 µm, compared to the inner side with 69 µm. Due to the extremely large number of grains included in the analysis, 112.583, the analysed variation over the wall thickness can be trusted. Figure 4-37 shows the disorientation distribution, same result as in the previous analyses with no LAGB and peaks for Σ3 and Σ9 boundaries.

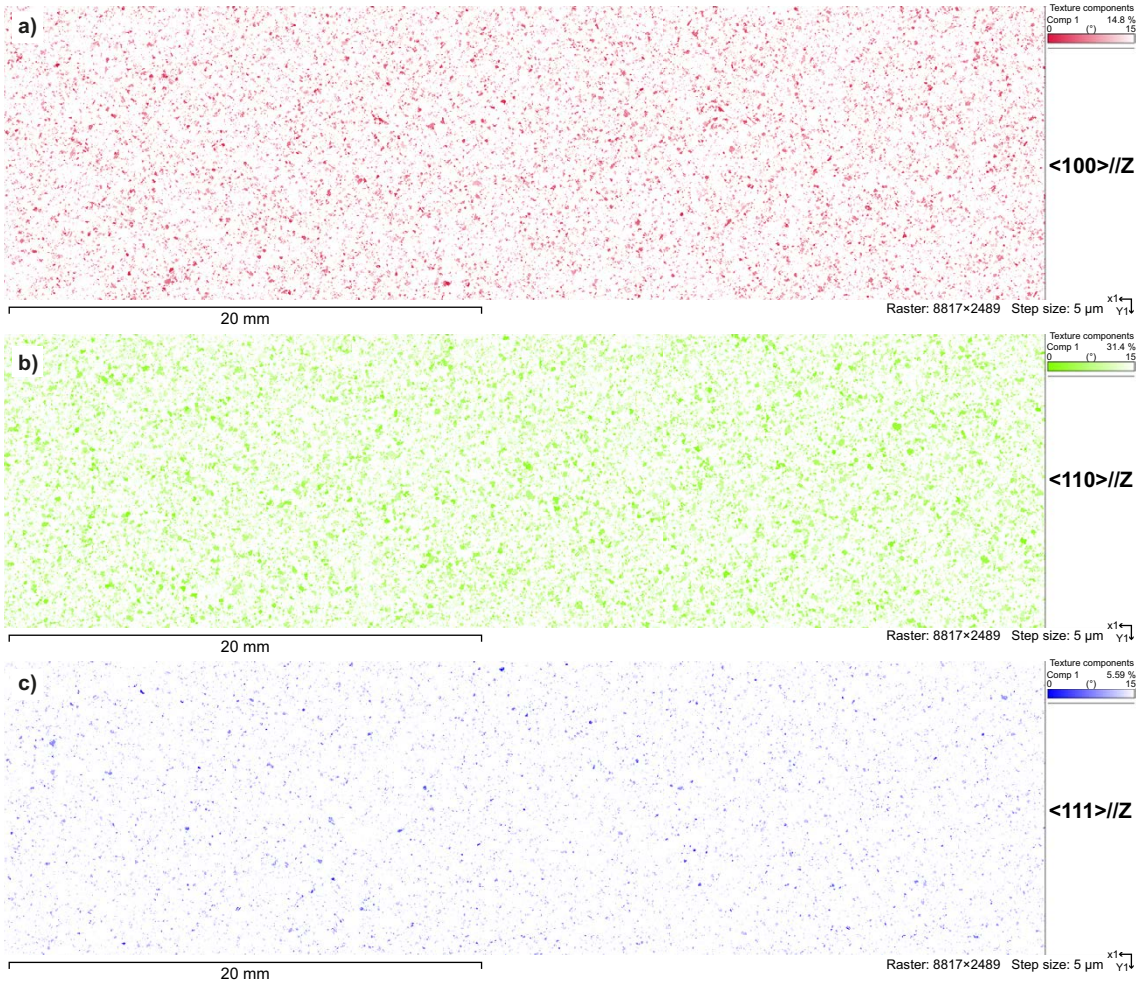

Figure 4-35. *Evaluation of fractions of close-packed planes parallel to the surface of the canister wall.*

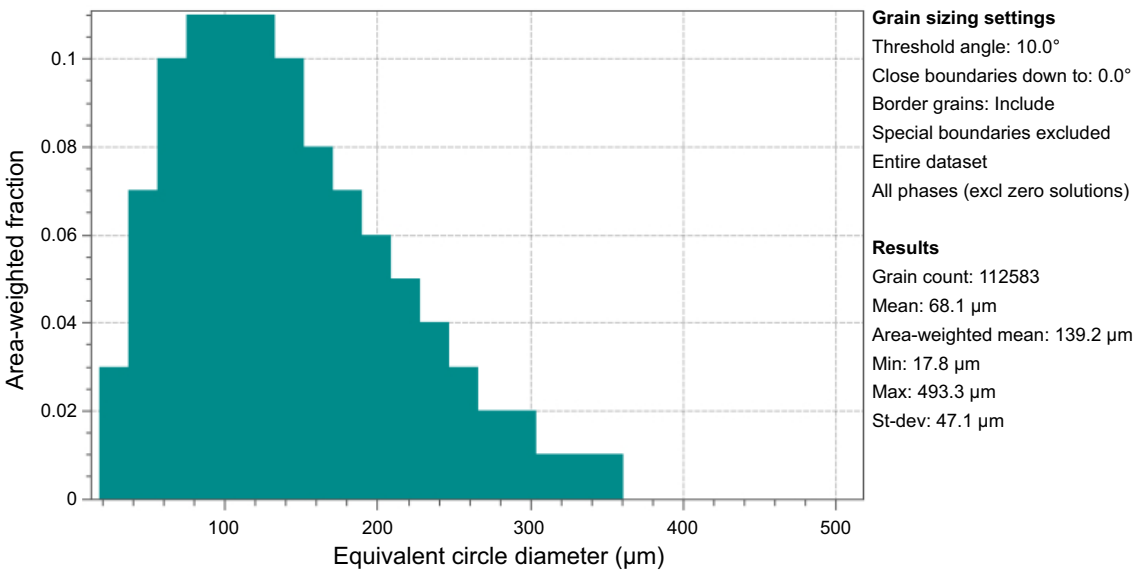

Figure 4-36. *Grain size distribution in canister T101 wall measured in the radial direction. 112 583 grains were included in the analysis.*

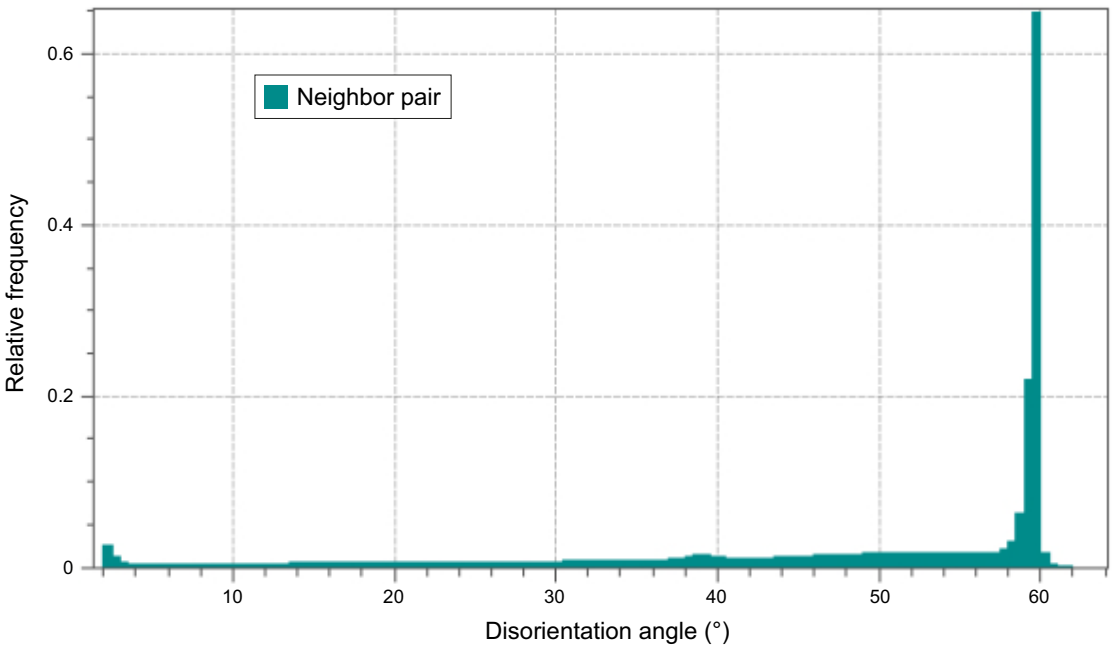

Figure 4-37. *Disorientation distribution in canister T101 wall measured in the radial direction.*

4.3.8 T101 Radial direction, Half depth, Fine microstructure (specimen #7, Table 4-2)

The radial section had the long side (X) parallel to the axial direction and short side parallel to the tangential direction. The acquisition area normal direction (Z) was parallel to the radial direction. The analysed surface origin was from the half depth in the tube wall (wall centre). Figure 4-38 shows the grains in the large area stitched EBSD map coloured with reference to the axial direction. Following the pattern from the previous analyses the cube orientation, <100> plane normal parallel to the axial direction were dominating the picture (red colour), but <111> grains (blue) were also present. Figure 4-39 shows the pole figures plotted with the acquisition axes as Y, Z and X. X was aligned to the axial direction. Z was equal to the radial direction and Y was aligned to the tangential direction. Z is also the thickness direction in the tube wall. The texture strength was 4.6 in this analysis and the strongest peak was the <100> planes in axial direction. The pole figures were in this case not as symmetric as the previous analysis from the surface region, which is also in agreement with previous results where the subsets at the centre were similar to the pole figures from the complete dataset. Texture strength did not change significantly from left to right.

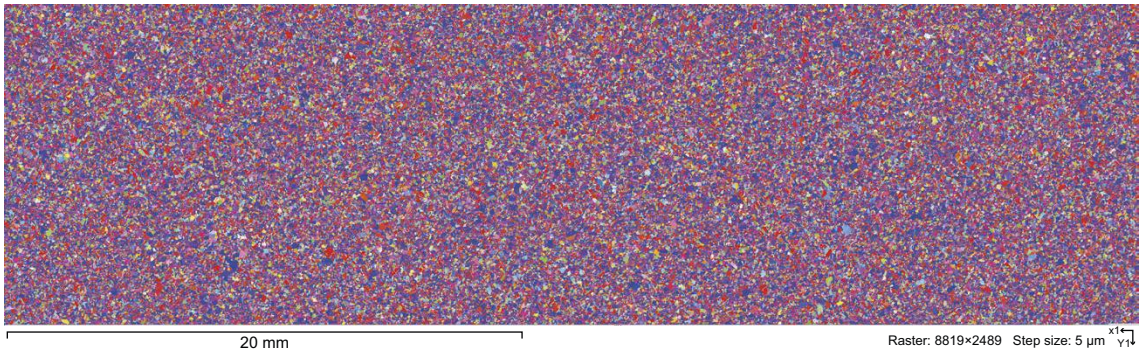

Figure 4-38. *EBSD analysis in radial direction in canister wall T101, half depth. The colours show the crystal orientation in the axial direction. The image is a rectangular subset from the original dataset.*

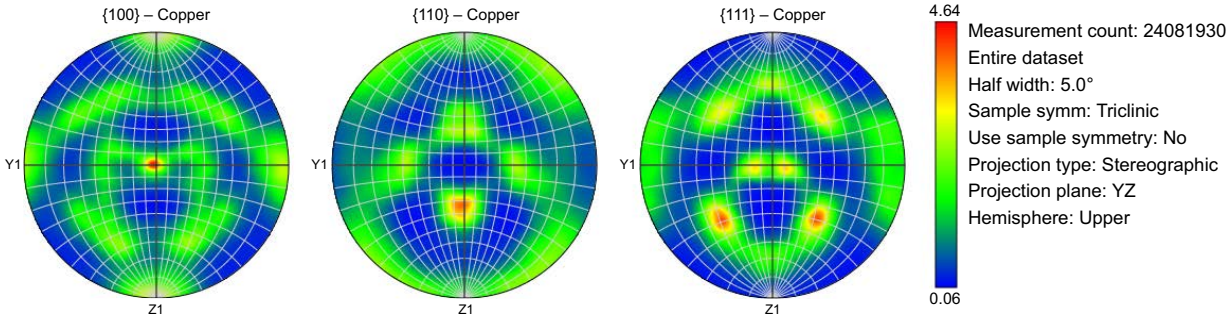

Figure 4-39. *Pole figure from the complete data set.*

The grain size distribution for the canister wall T101 measured on the radial section at the canister wall centre-line is shown in Figure 4-40. 114 302 grains were included in the analysis. The threshold for grain boundaries was set to 10° disorientation and the Σ3 and Σ9 twins were excluded in the analysis. The arithmetic mean diameter was 69 µm and the area weighted mean diameter was 130 µm, the largest grain had a diameter of 467 µm. Figure 4-41 shows the disorientation distribution, same result as in the previous analyses with no LAGB (dislocation built boundaries) and peaks for Σ3 and Σ9 boundaries.

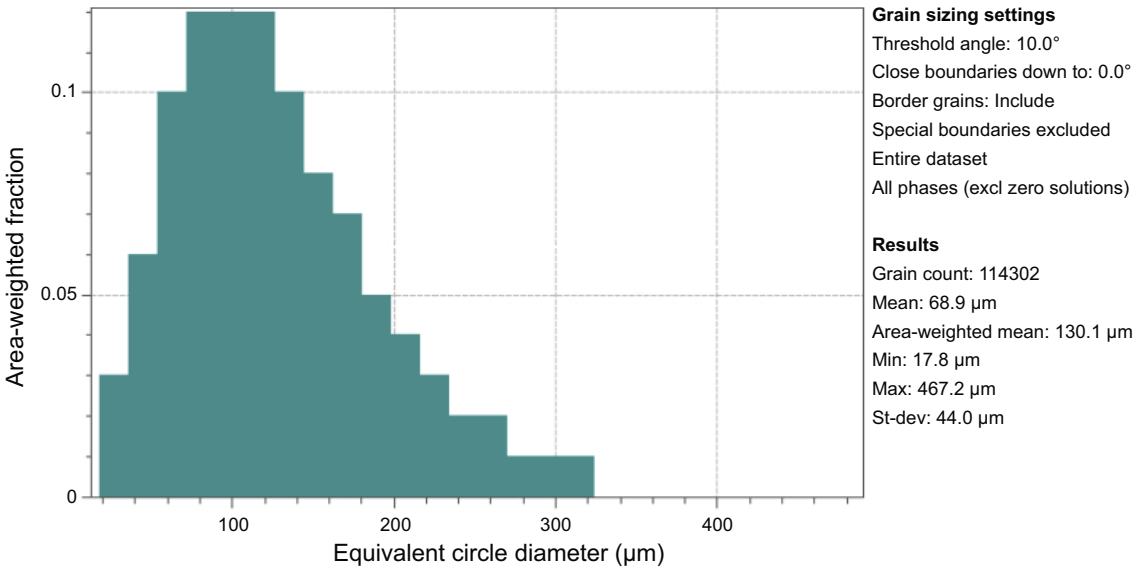

Figure 4-40. *Grain size distribution in canister T101 wall measured in the radial direction. 114 302 grains were included in the analysis.*

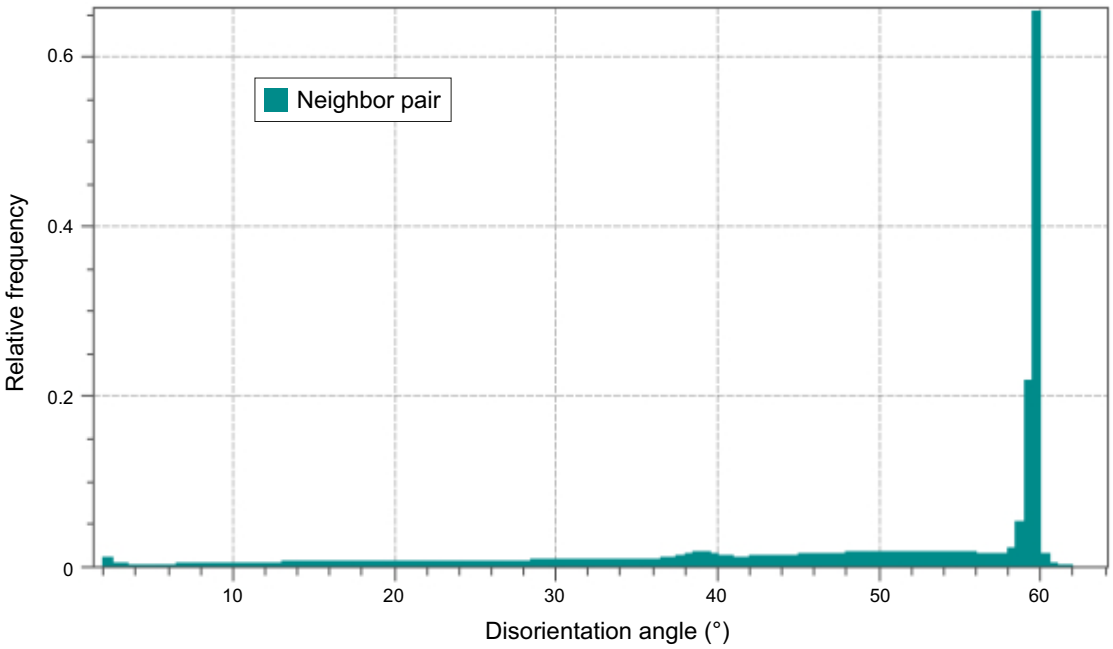

Figure 4-41. *Disorientation distribution in canister T101 wall measured in the radial direction. The surface was in this case from the centre of the canister wall.*

5 Discussion

The large amount of data available for the crystallographic texture, grain boundaries and grain size in the canisters is valuable for modelling of long-term properties. It can be used for improved understanding of the canister performance, but also for better understanding of how the production methods, the thermo-mechanical processing, affect the materials microstructure and in the end the materials mechanical as well as corrosion properties.

The models for diffusion that are used for prediction of long-term creep cannot (today) use all the detailed data presented here. This kind of data have not been available before but could now be used to improve the models. Further development of theories and models need to be done.

6 Conclusions

- The grain size was significantly larger in the top-sealing lid compared to the canister tube wall material. Arithmetic mean diameter values were around 70 µm in both materials, but the area-weighted mean was much larger in the lid material compared to the canister tube wall material, 200 µm compared to 130 µm. The large grains were larger and more frequent in the lid material.
- The canister wall was interpreted to be completely recrystallised in all positions that were analysed in this work based on the low fractions of LAGB found, the number fraction of LAGB (< 10°) was below 3 % in all positions except for one position close to the outer surface.
- The lid contained a higher fraction of LAGB (17 % in one direction and 24 % in the other, compared to 2–3 % in the walls). Also Σ9 boundaries were more frequent in the lid which also is connected to the non-recrystallised microstructure. Probably the plate material was recrystallised before the final forging operation, but the material was not heat treated after this which resulted in a certain degree of dislocations and deformation sub-structure.
- The texture was stronger in the canister tube wall material compared to the lid material. The texture was weak in the lid, around 2 times random. In the canister tube wall material, the texture was about 5 times random. Observe that texture strength is not a well-defined value, it is dependant of the method (in this case EBSD) and the parameters for calculating the pole figures, in this case 5° was chosen for the "half width".
- The outer surface showed a different texture compared to the other parts of the canister wall, see Figure 6-1. The analysed surface of specimen #5 was parallel to the outer surface and the position was close to the same surface (radial direction), compared to specimen #7 (half thickness) the texture was more symmetric and the <111> component in the axial direction was stronger. The fraction of large grains was also higher in this analysis (Table 4-2).
- Furthermore, at the outer surface, a higher fraction of <110> planes were parallel to the surface (31.4 %). The other main close packed planes were less frequent at the canister wall surface, <100> 15 % and <111> planes only 5.6 %.
- The top sealing lid material showed weaker texture and the difference between the fraction of planes parallel to the outer surface was smaller. Nevertheless, <111> planes were the most frequent with a fraction of 20.4 % parallel to the outer surface, then <100> planes were second most frequent (16.0 %) and <110> planes the least frequent ones (11.2 %).

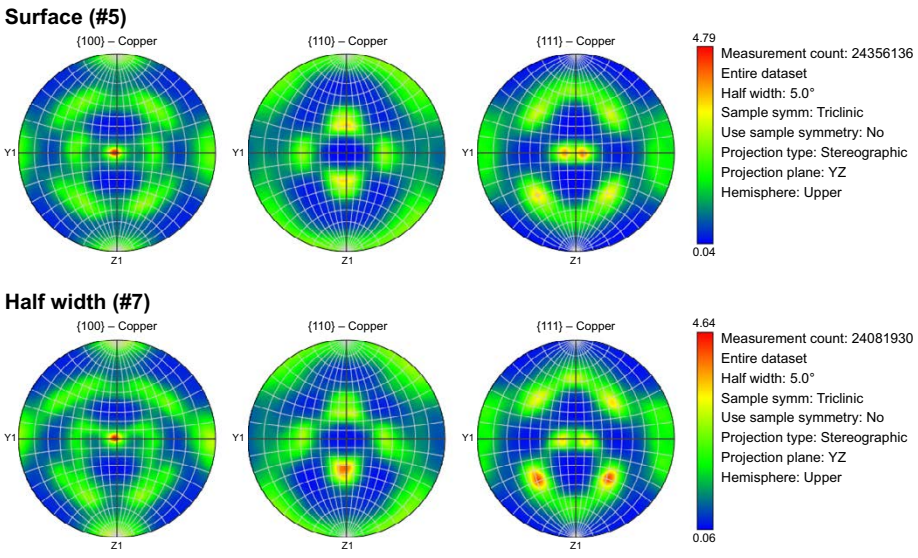

Figure 6-1. *Pole figures for specimen #5 (Figure 4-34) and specimen #7 (Figure 4-39).*

7 Suggested continued work

The original experimental plan included other positions and directions in the canister walls and lid of interest to fully understand the microstructure variations. These specimens were manufactured but not prepared for analysis. These specimens are available for analysis.

Corrosion testing for increased understanding of crystallographic texture and directions influence on corrosion rate.

References

SKB's (Svensk Kärnbränslehantering AB) publications can be found at www.skb.com/publications.

Azzi M, Szpunar J A, 2008. The Effects of Texture on the Corrosion Resistance of SS304 Stainless Steel. In Rollet A D (ed). Materials Processing and Texture. Hoboken, NJ: John Wiley & Sons.

Brandon P D, 1966. The structure of high-angle grain boundaries. Acta Metallurgica 14:11, 1479–1484.

Bunge H J, 1992. Texture Analysis in Materials Science: Mathematical Methods. Oxford: Butterworth-Heinemann.

Gottstein G, Shvindlerman L, 1999. Grain Boundary Migration in Metals. Boca Raton, FL: CRC Press.

Hagström J, Lindberg F, Hutchinson B, 2015. Modifiering av korngränsernas karaktär genom att variera processparametrarna i kallvalsade och glödgade bandmaterial av nickelbas superlegering X750. KIMAB-2015-109, Swerea KIMAB, Sweden. (In Swedish.)

Lindell D, Pettersson R, 2015. Crystallographic effects in corrosion of austenitic stainless steel 316L. Texture, Stress, and Microstructure 66:8, 727–732.

ISO, 2020. ISO 13067:2020. Microbeam analysis – Electron backscatter diffraction – Measurement of average grain size. Genève: International Organization for Standardization.

Lousada C M, Korzhavyi P A, 2022. Single vacancies at Σ5, Σ9 and Σ11 grain boundaries of copper and the geometrical factors that affect their site preference. Journal of Physics and Chemistry of Solids 169, 110833.

Mingard K P, Quested P N, Peck M S, 2012. Determination of grain size by EBSD Report on a round robin measurement of equiaxed Titanium. NPL REPORT MAT 56, National Physical Laboratory, UK.

Randle V, 2010. Grain boundary engineering: an overview after 25 years. Material Science and Technology 26, 253–261.

Sandström R, Lousada C M, 2021. The role of binding energies for phosphorus and sulphur at grain boundaries in copper Journal of Nuclear Materials 544, 152682.

Sutton B, Balluffi R W, 1998. Interfaces in Crystalline Materials. Oxford: Oxford University Press.

Thomsen K, Schmidt N H, Bewick A, Larsen K, Goulden J, 2013. Improving the Accuracy of Orientation Measurements using EBSD. Microscopy and Microanalysis, 19:S2, 724–725.

Trimby P, 2009. Analysis of the crystallographic signature of electron beam welds in Cu: implications for variations in etching characteristics. SKB R-09-18, Svensk Kärnbränslehantering AB.

Van Houtte P, 1987. On the Representation of Texture Functions of Cubic Metals in Euler Space. Texture, Stress, and Microstructure 7, 321546.

Appendix

List of CSL boundaries

All fractions of CSL boundaries in all materials, positions and directions

#1a. Canister T77 Wall, Axial Direction, Fine microstructure.

Boundary	Boundary Length, µm	Fraction of Grain Boundaries, %
Σ3 60° <111>	20 226 126	49.78
Σ5 36,87° <100>	89 897	0.22
Σ7 38,21° <111>	261 777	0.64
Σ9 38,94° <110>	1 053 394	2.59
Σ11 50,48° <110>	220 563	0.54
Σ13a 22,62° <100>	63 107	0.16
Σ13b 27,8° <111>	111 274	0.27
Σ13c 49,22° <322>	347 895	0.86
Σ15 48,19° <210>	123 970	0.31
Σ17a 28,07° <100>	28 523	0.07
Σ17b 61,93° <221>	155 397	0.38
Σ19a 26,53° <110>	81 284	0.20
Σ19b 46,83° <111>	67 975	0.17
Σ21a 21,79° <111>	70 299	0.17
Σ21b 44,4° <211>	105 761	0.26
Σ23 40,45° <311>	57 230	0.14
Σ25a 16,25° <100>	46 037	0.11
Σ25b 51,68° <331>	152 757	0.38
Σ27a 31,58° <110>	179 450	0.44
Σ27b 35,42° <210>	120 899	0.30
Σ29a 43,61° <100>	5 207	0.01
Σ29b 46,39° <221>	98 448	0.24
Σ31a 17,9° <111>	42 946	0.11
Σ31b 52,19° <211>	75 109	0.18
Σ33a 20,05° <110>	58 146	0.14
Σ33b 33,55° <311>	39 472	0.10
Σ33c 58,98° <110>	48 248	0.12
Σ35a 34,04° <211>	50 334	0.12
Σ35b 43,23° <331>	57 501	0.14
Σ37a 18,92° <100>	22 332	0.05
Σ37b 43,13° <310>	20 569	0.05
Σ37c 50,57° <111>	35 182	0.09
Σ39a 32,21° <111>	22 511	0.06
Σ39b 50,13° <321>	109 472	0.27
Σ41a 12,68° <100>	37 620	0.09
Σ41b 40,88° <210>	23 446	0.06
Σ41c 55,88° <110>	33 785	0.08
Σ43a 15,18° <111>	36 741	0.09
Σ43b 27,91° <210>	33 409	0.08
Σ43c 60,77° <332>	51 158	0.13
Σ45a 28,62° <311>	34 545	0.09
Σ45b 36,87° <221>	39 564	0.10
Σ45c 53,13° <221>	68 020	0.17
Σ47a 37,07° <331>	31 490	0.08
Σ47b 43,66° <320>	27 580	0.07
Σ49a 43,58° <111>	17 943	0.04
Σ49b 43,58° <511>	11 792	0.03

#1b. Canister T101 Wall, Axial Direction, Fine microstructure.

Boundary	Boundary Length, μm	Fraction of Grain Boundaries, %
Σ3 60° <111>	14 738 794	50.64
Σ5 36,87° <100>	59 923	0.21
Σ7 38,21° <111>	185 768	0.64
Σ9 38,94° <110>	680 758	2.34
Σ11 50,48° <110>	154 608	0.53
Σ13a 22,62° <100>	45 078	0.15
Σ13b 27,8° <111>	77 652	0.27
Σ13c 49,22° <322>	242 953	0.83
Σ15 48,19° <210>	86 516	0.30
Σ17a 28,07° <100>	19 770	0.07
Σ17b 61,93° <221>	110 110	0.38
Σ19a 26,53° <110>	59 170	0.20
Σ19b 46,83° <111>	48 425	0.17
Σ21a 21,79° <111>	51 210	0.18
Σ21b 44,4° <211>	73 710	0.25
Σ23 40,45° <311>	39 579	0.14
Σ25a 16,25° <100>	32 220	0.11
Σ25b 51,68° <331>	107 545	0.37
Σ27a 31,58° <110>	116 053	0.40
Σ27b 35,42° <210>	76 858	0.26
Σ29a 43,61° <100>	3 716	0.01
Σ29b 46,39° <221>	72 199	0.25
Σ31a 17,9° <111>	30 943	0.11
Σ31b 52,19° <211>	54 824	0.19
Σ33a 20,05° <110>	42 531	0.15
Σ33b 33,55° <311>	26 477	0.09
Σ33c 58,98° <110>	33 963	0.12
Σ35a 34,04° <211>	36 494	0.13
Σ35b 43,23° <331>	41 569	0.14
Σ37a 18,92° <100>	15 344	0.05
Σ37b 43,13° <310>	14 063	0.05
Σ37c 50,57° <111>	27 474	0.09
Σ39a 32,21° <111>	16 484	0.06
Σ39b 50,13° <321>	73 532	0.25
Σ41a 12,68° <100>	26 723	0.09
Σ41b 40,88° <210>	16 694	0.06
Σ41c 55,88° <110>	26 417	0.09
Σ43a 15,18° <111>	28 169	0.10
Σ43b 27,91° <210>	23 795	0.08
Σ43c 60,77° <332>	37 673	0.13
Σ45a 28,62° <311>	22 231	0.08
Σ45b 36,87° <221>	27 130	0.09
Σ45c 53,13° <221>	47 754	0.16
Σ47a 37,07° <331>	22 320	0.08
Σ47b 43,66° <320>	19 042	0.07
Σ49a 43,58° <111>	12 951	0.04
Σ49b 43,58° <511>	7 598	0.03

#2. Canister T101 Wall, Axial Direction, Coarse microstructure.

Boundary	Boundary Length, µm	Fraction of Grain Boundaries, %
Σ3 60° <111>	18 860 591	51.13
Σ5 36,87° <100>	77 282	0.21
Σ7 38,21° <111>	235 535	0.64
Σ9 38,94° <110>	833 184	2.26
Σ11 50,48° <110>	193 164	0.52
Σ13a 22,62° <100>	54 496	0.15
Σ13b 27,8° <111>	95 645	0.26
Σ13c 49,22° <322>	311 186	0.84
Σ15 48,19° <210>	107 613	0.29
Σ17a 28,07° <100>	23 236	0.06
Σ17b 61,93° <221>	142 251	0.39
Σ19a 26,53° <110>	72 099	0.20
Σ19b 46,83° <111>	63 610	0.17
Σ21a 21,79° <111>	64 074	0.17
Σ21b 44,4° <211>	93 043	0.25
Σ23 40,45° <311>	47 684	0.13
Σ25a 16,25° <100>	38 294	0.10
Σ25b 51,68° <331>	129 782	0.35
Σ27a 31,58° <110>	142 503	0.39
Σ27b 35,42° <210>	92 513	0.25
Σ29a 43,61° <100>	4 646	0.01
Σ29b 46,39° <221>	86 665	0.23
Σ31a 17,9° <111>	41 429	0.11
Σ31b 52,19° <211>	66 712	0.18
Σ33a 20,05° <110>	54 676	0.15
Σ33b 33,55° <311>	34 620	0.09
Σ33c 58,98° <110>	42 575	0.12
Σ35a 34,04° <211>	43 589	0.12
Σ35b 43,23° <331>	52 146	0.14
Σ37a 18,92° <100>	20 343	0.06
Σ37b 43,13° <310>	15 930	0.04
Σ37c 50,57° <111>	33 668	0.09
Σ39a 32,21° <111>	18 945	0.05
Σ39b 50,13° <321>	94 943	0.26
Σ41a 12,68° <100>	34 580	0.09
Σ41b 40,88° <210>	18 583	0.05
Σ41c 55,88° <110>	33 232	0.09
Σ43a 15,18° <111>	34 393	0.09
Σ43b 27,91° <210>	30 116	0.08
Σ43c 60,77° <332>	51 296	0.14
Σ45a 28,62° <311>	28 534	0.08
Σ45b 36,87° <221>	34 482	0.09
Σ45c 53,13° <221>	61 307	0.17
Σ47a 37,07° <331>	28 344	0.08
Σ47b 43,66° <320>	25 116	0.07
Σ49a 43,58° <111>	16 379	0.04
Σ49b 43,58° <511>	10 085	0.03

#3. Canister T101 Wall, Tangential Direction, Fine microstructure.

Boundary	Boundary Length, µm	Fraction of Grain Boundaries, %
Σ3 60° <111>	16 978 297	49.86
Σ5 36,87° <100>	71 750	0.21
Σ7 38,21° <111>	218 679	0.64
Σ9 38,94° <110>	793 550	2.33
Σ11 50,48° <110>	188 877	0.55
Σ13a 22,62° <100>	50 408	0.15
Σ13b 27,8° <111>	90 769	0.27
Σ15 48,19° <210>	104 077	0.31
Σ17a 28,07° <100>	22 249	0.07
Σ17b 61,93° <221>	128 512	0.38
Σ19a 26,53° <110>	67 106	0.20
Σ19b 46,83° <111>	58 187	0.17
Σ21a 21,79° <111>	60 443	0.18
Σ21b 44,4° <211>	83 237	0.24
Σ23 40,45° <311>	46 052	0.14
Σ25a 16,25° <100>	37 719	0.11
Σ25b 51,68° <331>	124 955	0.37
Σ27a 31,58° <110>	135 110	0.40
Σ27b 35,42° <210>	91 042	0.27
Σ29a 43,61° <100>	3 853	0.01
Σ29b 46,39° <221>	82 112	0.24
Σ31a 17,9° <111>	38 614	0.11
Σ31b 52,19° <211>	63 069	0.19
Σ33a 20,05° <110>	49 388	0.15
Σ33b 33,55° <311>	32 843	0.10
Σ33c 58,98° <110>	41 766	0.12
Σ35a 34,04° <211>	41 897	0.12
Σ35b 43,23° <331>	48 073	0.14
Σ37a 18,92° <100>	18 531	0.05
Σ37b 43,13° <310>	15 256	0.04
Σ37c 50,57° <111>	32 585	0.10
Σ39a 32,21° <111>	18 969	0.06
Σ39b 50,13° <321>	90 229	0.26
Σ41a 12,68° <100>	30 271	0.09
Σ41b 40,88° <210>	19 521	0.06
Σ41c 55,88° <110>	31 905	0.09
Σ43a 15,18° <111>	32 007	0.09
Σ43b 27,91° <210>	28 176	0.08
Σ43c 60,77° <332>	43 986	0.13
Σ45a 28,62° <311>	28 171	0.08
Σ45b 36,87° <221>	31 488	0.09
Σ45c 53,13° <221>	56 994	0.17
Σ47a 37,07° <331>	27 575	0.08
Σ47b 43,66° <320>	23 433	0.07
Σ49a 43,58° <111>	15 769	0.05
Σ49b 43,58° <511>	9 704	0.03
Σ49c 49,22° <322>	38 551	0.11

#4. Canister T77 Wall, Tangential Direction, Coarse microstructure.

Boundary	Boundary Length, µm	Fraction of Grain Boundaries per Phase, %
Σ3 60° <111>	19432988	49.98
Σ5 36,87° <100>	87355	0.22
Σ7 38,21° <111>	245721	0.63
Σ9 38,94° <110>	984865	2.53
Σ11 50,48° <110>	213482	0.55
Σ13a 22,62° <100>	60036	0.15
Σ13b 27,8° <111>	108749	0.28
Σ13c 49,22° <322>	329530	0.85
Σ15 48,19° <210>	120386	0.31
Σ17a 28,07° <100>	27759	0.07
Σ17b 61,93° <221>	146260	0.38
Σ19a 26,53° <110>	76670	0.20
Σ19b 46,83° <111>	63624	0.16
Σ21a 21,79° <111>	68854	0.18
Σ21b 44,4° <211>	99339	0.26
Σ23 40,45° <311>	53784	0.14
Σ25a 16,25° <100>	42421	0.11
Σ25b 51,68° <331>	141378	0.36
Σ27a 31,58° <110>	173249	0.45
Σ27b 35,42° <210>	114899	0.30
Σ29a 43,61° <100>	5041	0.01
Σ29b 46,39° <221>	93135	0.24
Σ31a 17,9° <111>	44983	0.12
Σ31b 52,19° <211>	71581	0.18
Σ33a 20,05° <110>	55125	0.14
Σ33b 33,55° <311>	37081	0.10
Σ33c 58,98° <110>	48654	0.13
Σ35a 34,04° <211>	48206	0.12
Σ35b 43,23° <331>	55561	0.14
Σ37a 18,92° <100>	20636	0.05
Σ37b 43,13° <310>	20034	0.05
Σ37c 50,57° <111>	35110	0.09
Σ39a 32,21° <111>	20989	0.05
Σ39b 50,13° <321>	100248	0.26
Σ41a 12,68° <100>	34472	0.09
Σ41b 40,88° <210>	22697	0.06
Σ41c 55,88° <110>	34372	0.09
Σ43a 15,18° <111>	35866	0.09
Σ43b 27,91° <210>	31880	0.08
Σ43c 60,77° <332>	51514	0.13
Σ45a 28,62° <311>	32216	0.08
Σ45b 36,87° <221>	36434	0.09
Σ45c 53,13° <221>	65803	0.17
Σ47a 37,07° <331>	30315	0.08
Σ47b 43,66° <320>	25778	0.07
Σ49a 43,58° <111>	18987	0.05
Σ49b 43,58° <511>	11537	0.03

#5. Canister T101 Wall, Radial Direction, Fine microstructure, Half.

Boundary	Boundary Length, µm	Fraction of Grain Boundaries, %
Σ3 60° <111>	16 211 452	51.18
Σ5 36,87° <100>	70 923	0.22
Σ7 38,21° <111>	198 815	0.63
Σ9 38,94° <110>	773 078	2.44
Σ11 50,48° <110>	169 115	0.53
Σ13a 22,62° <100>	45 241	0.14
Σ13b 27,8° <111>	85 620	0.27
Σ15 48,19° <210>	94 600	0.30
Σ17a 28,07° <100>	21 163	0.07
Σ17b 61,93° <221>	120 820	0.38
Σ19a 26,53° <110>	62 015	0.20
Σ19b 46,83° <111>	52 995	0.17
Σ21a 21,79° <111>	55 541	0.18
Σ21b 44,4° <211>	77 747	0.25
Σ23 40,45° <311>	44 550	0.14
Σ25a 16,25° <100>	32 281	0.10
Σ25b 51,68° <331>	114 139	0.36
Σ27a 31,58° <110>	128 844	0.41
Σ27b 35,42° <210>	84 201	0.27
Σ29a 43,61° <100>	4 404	0.01
Σ29b 46,39° <221>	75 769	0.24
Σ31a 17,9° <111>	32 898	0.10
Σ31b 52,19° <211>	57 423	0.18
Σ33a 20,05° <110>	44 171	0.14
Σ33b 33,55° <311>	30 752	0.10
Σ33c 58,98° <110>	37 998	0.12
Σ35a 34,04° <211>	38 974	0.12
Σ35b 43,23° <331>	46 695	0.15
Σ37a 18,92° <100>	15 147	0.05
Σ37b 43,13° <310>	16 064	0.05
Σ37c 50,57° <111>	29 789	0.09
Σ39a 32,21° <111>	16 689	0.05
Σ39b 50,13° <321>	83 442	0.26
Σ41a 12,68° <100>	25 950	0.08
Σ41b 40,88° <210>	17 693	0.06
Σ41c 55,88° <110>	27 900	0.09
Σ43a 15,18° <111>	26 142	0.08
Σ43b 27,91° <210>	25 867	0.08
Σ43c 60,77° <332>	39 498	0.12
Σ45a 28,62° <311>	25 334	0.08
Σ45b 36,87° <221>	28 311	0.09
Σ45c 53,13° <221>	51 930	0.16
Σ47a 37,07° <331>	25 385	0.08
Σ47b 43,66° <320>	20 416	0.06
Σ49a 43,58° <111>	13 889	0.04
Σ49b 43,58° <511>	9 625	0.03
Σ49c 49,22° <322>	36 663	0.12

#6. Canister T77 Wall, Radial Direction, Coarse microstructure.

Boundary	Boundary Length, µm	Fraction of Grain Boundaries per Phase, %
Σ3 60° <111>	20623416	50.20
Σ5 36,87° <100>	96562	0.24
Σ7 38,21° <111>	263279	0.64
Σ9 38,94° <110>	1085084	2.64
Σ11 50,48° <110>	219081	0.53
Σ13a 22,62° <100>	63708	0.16
Σ13b 27,8° <111>	115579	0.28
Σ15 48,19° <210>	131277	0.32
Σ17a 28,07° <100>	29330	0.07
Σ17b 61,93° <221>	150359	0.37
Σ19a 26,53° <110>	84443	0.21
Σ19b 46,83° <111>	67258	0.16
Σ21a 21,79° <111>	71383	0.17
Σ21b 44,4° <211>	105583	0.26
Σ23 40,45° <311>	60657	0.15
Σ25a 16,25° <100>	42947	0.10
Σ25b 51,68° <331>	149389	0.36
Σ27a 31,58° <110>	185366	0.45
Σ27b 35,42° <210>	127526	0.31
Σ29a 43,61° <100>	5610	0.01
Σ29b 46,39° <221>	97324	0.24
Σ31a 17,9° <111>	43657	0.11
Σ31b 52,19° <211>	74279	0.18
Σ33a 20,05° <110>	59641	0.15
Σ33b 33,55° <311>	42970	0.10
Σ33c 58,98° <110>	48192	0.12
Σ35a 34,04° <211>	50643	0.12
Σ35b 43,23° <331>	59335	0.14
Σ37a 18,92° <100>	22411	0.05
Σ37b 43,13° <310>	21430	0.05
Σ37c 50,57° <111>	35750	0.09
Σ39a 32,21° <111>	23644	0.06
Σ39b 50,13° <321>	110412	0.27
Σ41a 12,68° <100>	35385	0.09
Σ41b 40,88° <210>	25242	0.06
Σ41c 55,88° <110>	35517	0.09
Σ43a 15,18° <111>	35721	0.09
Σ43b 27,91° <210>	35422	0.09
Σ43c 60,77° <332>	50171	0.12
Σ45a 28,62° <311>	33869	0.08
Σ45b 36,87° <221>	38206	0.09
Σ45c 53,13° <221>	67294	0.16
Σ47a 37,07° <331>	32944	0.08
Σ47b 43,66° <320>	28264	0.07
Σ49a 43,58° <111>	17232	0.04
Σ49b 43,58° <511>	13807	0.03
Σ49c 49,22° <322>	46399	0.11

#7. Canister T101 Wall, Radial Direction, Fine microstructure, Surface.

Boundary	Boundary Length, µm	Fraction of Grain Boundaries, %
Σ3 60° <111>	15 544 059	53.71
Σ5 36,87° <100>	56 949	0.20
Σ7 38,21° <111>	166 313	0.57
Σ9 38,94° <110>	625 853	2.16
Σ11 50,48° <110>	161 070	0.56
Σ13a 22,62° <100>	41 338	0.14
Σ13b 27,8° <111>	74 353	0.26
Σ15 48,19° <210>	79 260	0.27
Σ17a 28,07° <100>	18 912	0.07
Σ17b 61,93° <221>	106 707	0.37
Σ19a 26,53° <110>	58 720	0.20
Σ19b 46,83° <111>	43 845	0.15
Σ21a 21,79° <111>	45 958	0.16
Σ21b 44,4° <211>	69 281	0.24
Σ23 40,45° <311>	36 907	0.13
Σ25a 16,25° <100>	27 665	0.10
Σ25b 51,68° <331>	100 241	0.35
Σ27a 31,58° <110>	91 354	0.32
Σ27b 35,42° <210>	56 429	0.19
Σ29a 43,61° <100>	3 193	0.01
Σ29b 46,39° <221>	64 965	0.22
Σ31a 17,9° <111>	28 532	0.10
Σ31b 52,19° <211>	49 050	0.17
Σ33a 20,05° <110>	40 748	0.14
Σ33b 33,55° <311>	26 114	0.09
Σ33c 58,98° <110>	36 997	0.13
Σ35a 34,04° <211>	34 136	0.12
Σ35b 43,23° <331>	39 038	0.13
Σ37a 18,92° <100>	12 857	0.04
Σ37b 43,13° <310>	12 724	0.04
Σ37c 50,57° <111>	24 990	0.09
Σ39a 32,21° <111>	14 256	0.05
Σ39b 50,13° <321>	71 485	0.25
Σ41a 12,68° <100>	23 502	0.08
Σ41b 40,88° <210>	15 946	0.06
Σ41c 55,88° <110>	26 426	0.09
Σ43a 15,18° <111>	25 889	0.09
Σ43b 27,91° <210>	22 124	0.08
Σ43c 60,77° <332>	37 850	0.13
Σ45a 28,62° <311>	22 229	0.08
Σ45b 36,87° <221>	24 290	0.08
Σ45c 53,13° <221>	44 843	0.15
Σ47a 37,07° <331>	23 688	0.08
Σ47b 43,66° <320>	18 718	0.06
Σ49a 43,58° <111>	11 574	0.04
Σ49b 43,58° <511>	8 098	0.03
Σ49c 49,22° <322>	30 145	0.10

#8. Top-sealing lid, Axial Direction, Coarse microstructure, Half depth.

Boundary	Boundary Length, µm	Fraction of CSL Grain Boundaries, %
Σ3 60° <111>	11 784 209	51.96
Σ5 36,87° <100>	71 951	0.32
Σ7 38,21° <111>	102 638	0.45
Σ9 38,94° <110>	1 204 954	5.31
Σ11 50,48° <110>	109 341	0.48
Σ13a 22,62° <100>	30 723	0.14
Σ13b 27,8° <111>	48 393	0.21
Σ15 48,19° <210>	74 820	0.33
Σ17a 28,07° <100>	17 065	0.08
Σ17b 61,93° <221>	67 212	0.30
Σ19a 26,53° <110>	58 431	0.26
Σ19b 46,83° <111>	27 187	0.12
Σ21a 21,79° <111>	29 766	0.13
Σ21b 44,4° <211>	56 144	0.25
Σ23 40,45° <311>	40 192	0.18
Σ25a 16,25° <100>	19 244	0.08
Σ25b 51,68° <331>	69 350	0.31
Σ27a 31,58° <110>	192 689	0.85
Σ27b 35,42° <210>	180 256	0.79
Σ29a 43,61° <100>	5 498	0.02
Σ29b 46,39° <221>	44 886	0.20
Σ31a 17,9° <111>	17 037	0.08
Σ31b 52,19° <211>	37 715	0.17
Σ33a 20,05° <110>	21 381	0.09
Σ33b 33,55° <311>	23 657	0.10
Σ33c 58,98° <110>	24 246	0.11
Σ35a 34,04° <211>	27 896	0.12
Σ35b 43,23° <331>	28 976	0.13
Σ37a 18,92° <100>	10 103	0.04
Σ37b 43,13° <310>	16 103	0.07
Σ37c 50,57° <111>	15 757	0.07
Σ39a 32,21° <111>	9 987	0.04
Σ39b 50,13° <321>	50 685	0.22
Σ41a 12,68° <100>	13 517	0.06
Σ41b 40,88° <210>	18 538	0.08
Σ41c 55,88° <110>	16 593	0.07
Σ43a 15,18° <111>	13 060	0.06
Σ43b 27,91° <210>	19 800	0.09
Σ43c 60,77° <332>	36 669	0.16
Σ45a 28,62° <311>	17 664	0.08
Σ45b 36,87° <221>	18 825	0.08
Σ45c 53,13° <221>	31 822	0.14
Σ47a 37,07° <331>	17 136	0.08
Σ47b 43,66° <320>	16499	0.07
Σ49a 43,58° <111>	7804	0.03
Σ49b 43,58° <511>	10665	0.05
Σ49c 49,22° <322>	22414	0.10

#9. Top-sealing lid Tangential Direction, Coarse microstructure.

Boundary	Boundary Length, µm	Fraction of Grain Boundaries per Phase, %
Σ3 60° <111>	15 114 499	48.53
Σ5 36,87° <100>	98 133	0.32
Σ7 38,21° <111>	159 358	0.51
Σ9 38,94° <110>	1 568 045	5.03
Σ11 50,48° <110>	161 418	0.52
Σ13a 22,62° <100>	45 740	0.15
Σ13b 27,8° <111>	79 178	0.25
Σ13c 49,22° <322>	249 517	0.80
Σ15 48,19° <210>	107 257	0.34
Σ17a 28,07° <100>	23 859	0.08
Σ17b 61,93° <221>	99 334	0.32
Σ19a 26,53° <110>	88 102	0.28
Σ19b 46,83° <111>	42 243	0.14
Σ21a 21,79° <111>	47 866	0.15
Σ21b 44,4° <211>	80 528	0.26
Σ23 40,45° <311>	57 524	0.18
Σ25a 16,25° <100>	31 505	0.10
Σ25b 51,68° <331>	105 029	0.34
Σ27a 31,58° <110>	248 460	0.80
Σ27b 35,42° <210>	235 516	0.76
Σ29a 43,61° <100>	6 768	0.02
Σ29b 46,39° <221>	67 241	0.22
Σ31a 17,9° <111>	27 663	0.09
Σ31b 52,19° <211>	54 447	0.17
Σ33a 20,05° <110>	30 910	0.10
Σ33b 33,55° <311>	34 829	0.11
Σ33c 58,98° <110>	35 570	0.11
Σ35a 34,04° <211>	40 618	0.13
Σ35b 43,23° <331>	44 426	0.14
Σ37a 18,92° <100>	15 220	0.05
Σ37b 43,13° <310>	22 600	0.07
Σ37c 50,57° <111>	24 186	0.08
Σ39a 32,21° <111>	15 533	0.05
Σ39b 50,13° <321>	80 646	0.26
Σ41a 12,68° <100>	22 923	0.07
Σ41b 40,88° <210>	27 967	0.09
Σ41c 55,88° <110>	23 778	0.08
Σ43a 15,18° <111>	21 235	0.07
Σ43b 27,91° <210>	29 126	0.09
Σ43c 60,77° <332>	50 457	0.16
Σ45a 28,62° <311>	27 614	0.09
Σ45b 36,87° <221>	28 214	0.09
Σ45c 53,13° <221>	48 429	0.16
Σ47a 37,07° <331>	25 624	0.08
Σ47b 43,66° <320>	24 207	0.08
Σ49a 43,58° <111>	10 367	0.03
Σ49b 43,58° <511>	14 502	0.05

Arkitektkopia AB, Bromma, 2023

SKB is responsible for managing spent nuclear fuel and radioactive waste produced by the Swedish nuclear power plants such that man and the environment are protected in the near and distant future.

skb.se